Hydrol. Earth Syst. Sci. Discuss., 9, 541–594, 2012
www.hydrol-earth-syst-sci-discuss.net/9/541/2012/
doi:10.5194/hessd-9-541-2012

Hydrology and Earth System Sciences Discussions

Climatic and geologic controls on suspended sediment flux in the Sutlej River Valley, western Himalaya

H. Wulf[1], B. Bookhagen[2], and D. Scherler[1]

[1]Department of Earth and Environmental Science, Potsdam University, Potsdam, Germany
[2]Department of Geography, University of California, Santa Barbara, USA

Received: 19 December 2011 – Accepted: 25 December 2011 – Published: 11 January 2012

Correspondence to: H. Wulf (hendrik.wulf@uni-potsdam.de)

Published by Copernicus Publications on behalf of the European Geosciences Union.

Abstract

The sediment flux through Himalayan rivers directly impacts water quality and is important for sustaining agriculture as well as maintaining drinking-water and hydropower generation. Despite the recent increase in demand for these resources, little is known about the triggers and sources of extreme sediment flux events, which lower water quality and account for extensive hydropower reservoir filling and turbine abrasion. Here, we present a comprehensive analysis of the spatiotemporal trends in suspended sediment flux based on daily data during the past decade (2001–2009) from four sites along the Sutlej River and from four of its main tributaries. In conjunction with satellite data depicting rainfall and snow cover, air temperature, earthquake records, and Schmidt hammer rock strength measurements, we infer climatic and geologic controls of peak suspended sediment concentration (SSC) events. Our study identifies three key findings: First, peak SSC events (≥99th SSC percentile) coincide frequently (57–80 %) with heavy rainstorms and account for about 30 % of the suspended sediment flux in the semi-arid to arid interior of the orogen. Second, we observe an increase of suspended sediment flux from the Tibetan Plateau to the Himalayan front at mean annual timescales. This sediment-flux gradient suggests that averaged, modern erosion in the western Himalaya is most pronounced at frontal regions, which are characterized by high monsoonal rainfall and thick soil cover. Third, in seven of eight catchments we find an anticlockwise hysteresis loop of annual sediment flux, which appears to be related to enhanced glacial sediment evacuation during late summer. Our analysis emphasizes the importance of unconsolidated sediments in the high-elevation sector that can easily be mobilized by hydrometeorological events and higher glacial-meltwater contributions.

HESSD

9, 541–594, 2012

1 Introduction

Pronounced erosion in the Himalaya delivers large amounts of sediment to the Indus and the Ganges-Brahmaputra river systems, which build up the worlds two largest submarine fans in the Arabian Sea (up to 10 km thickness) (Clift et al., 2001) and the Bay of Bengal (up to 16.5 km thickness) (Curray et al., 2003), respectively. The sediment loads of these rivers (Indus: 250 Mt yr^{-1}, Ganges: 520 Mt yr^{-1}, Brahmaputra: 540 Mt yr^{-1}) rank among the highest in the world and contribute ~10 % to the global sediments reaching the oceans (Milliman and Syvitski, 1992). Knowledge of the magnitude and distribution of orogenic erosion rates as well as the operating processes is crucial for understanding how these landscapes evolve (Molnar and England, 1990; Small and Anderson, 1995) and how erosion might affect active tectonics (Burbank et al., 1996; Clift et al., 2008; Thiede et al., 2004, 2009; Wobus et al., 2005) and global climatic changes (Raymo et al., 1988; Raymo and Ruddiman, 1992). Furthermore, quantifying the spatiotemporal patterns and variation of fluvial sediment flux is important, because it affects the lifetime of hydropower reservoirs and abrades hydropower turbines (e.g. Singh et al., 2003).

High topographic relief, steep river profiles, and elevated stream power all indicate high erosion rates throughout the Himalaya (Finlayson et al., 2002; Vance et al., 2003). Most authors agree that rapid rock uplift and heavy monsoonal precipitation lead to rapid fluvial incision and hillslope mass wasting along the southern front of the Himalaya (e.g. Galy and France-Lanord, 2001; Hodges et al., 2004; Thiede et al., 2004). Particularly the eastern and western syntaxes are areas of high exhumation and erosion (1–10 mm yr^{-1}) (Burbank et al., 1996; Burg et al., 1998; Finnegan et al., 2008; Stewart et al., 2008; Zeitler et al., 2001). In contrast, on the orographically shielded Tibetan Plateau, erosion rates are significantly lower (<0.03 mm yr^{-1}), due to lower rainfall amounts and lower topographic relief (Lal et al., 2003). However, several studies suggest that during active monsoon phases strong convective cells can migrate across the orographic barrier and result in heavy rainfall events, which can mobilize enormous

HESSD
9, 541–594, 2012
Climatic controls on suspended sediment flux in the Sutlej River Valley
H. Wulf et al.

amounts of sediments in the orogen's interior (e.g. Bookhagen, 2010; Bookhagen et al., 2005; Craddock et al., 2007; Wulf et al., 2010).

Long-term (>10^3 yr) rates of erosion and models of landscape evolution are typically based on thermochronological (e.g. Reiners et al., 2005) and cosmogenic nuclide data (e.g. Bierman, 1994; Bookhagen and Strecker, 2012; von Blanckenburg, 2005). More direct measurements of fluvial sediment yields, spanning years to decades, can be inferred from sediment accumulation rates in reservoirs (sediment trapping), or from measurements of suspended sediment and bedload fluxes in rivers (sediment gauging) (Meade, 1988; Wulf et al., 2010). Although fluvial sediment measurements do not reliable record low-frequency, high-intensity events and rarely include the bedload fraction, they provide valuable insights into the behavior of rivers and their coupling to weather and climate (e.g. Wolman and Miller, 1960). This coupling between climate and rivers also elucidates the impact of climate change on surface erosion and fluvial sediment flux, as increasing temperatures cause pronounced environmental changes in the Himalayan region (IPCC, 2007).

In this study, we analyze daily river discharge and suspended sediment concentration (SSC) data from the Sutlej River Valley in the western Himalaya to study the sediment flux (i.e. discharge multiplied by SSC) characteristics in different geologic and climatic regions. We compare the sediment flux data from four sites along the main stem of the Sutlej and from four of its largest tributaries with remotely sensed rainfall and snow cover data, as well as air temperature and earthquake records, and rock-strength measurements to investigate the climatic and geologic controls on low-frequency, high-magnitude sediment discharges. Previous research shows that such peak events often account for a large fraction of the sediment budget (e.g. Barnard et al., 2001; Bookhagen et al., 2005; Henck et al., 2010; Kirchner et al., 2001; Wulf et al., 2010). In a final step we compare the new data with published sediment flux data from across the Himalaya to identify spatial patterns and first-order controls on sediment transport.

HESSD
9, 541–594, 2012

2 Geographic, climatic, and geologic setting

2.1 Geographic setting

The Sutlej River is the largest tributary of the Indus River and drains the third largest catchment area in the Himalaya (ca. 55 000 km^2 above 500 m a.s.l.). Approximately two-thirds of this area are located in China and drain the Zhada basin, which stretches NW–SE between the southern edge of the Tibetan Plateau and the Mount Kailash range. To the west, the Indian part of the Sutlej Valley covers a wide range of elevations between the Indo-Gangetic Plains (400 m a.s.l. – above sea level, asl) and the Himalayan Crest (6400 m a.s.l.) (Fig. 1). The catchment-average altitude is 4400 m a.s.l. More than 80 % of the catchment area is located at >4000 m asl and has virtually no vegetation cover (Fig. 1a). The lower part of the catchment area (<4000 m a.s.l.) is located at the monsoon-impacted southern front of the Himalaya, where vegetation is lush and dense. Therefore the primary land cover in the Sutlej Valley is bare ground (81.2 %), next to trees and shrubs (7.2 %), cultivated areas (6.8 %), glaciers (3.7 %), and lakes (1.1 %) (FAO, 2009). Hence, developed soils cover only a small fraction (<15 %), mostly in the lower part of the Sutlej Valley. Glacial cover is particularly dense at the Himalayan Crest, where snowfall is highest (e.g. Singh and Kumar, 1997). As a result, river runoff dominated by snow- and glacial-melt from the high, orographically-shielded Himalayan Crest is comparable in magnitude to the Himalayan Front, which is dominated by monsoonal rainfall (Bookhagen and Burbank, 2010).

Throughout this study we distinguish between the Himalayan Front, the Himalayan Crest, and the Tibetan Plateau region based on topographic and climatic characteristics (Fig. 1b). The Himalayan Front marks the area between the Indo-Gangetic Plains and the high Himalayan peaks, and is characterized by high monsoonal rainfall and dense vegetation at elevations <3500 m. The Ganvi catchment is part of this region, although somewhat set back into the orogen due to the broad and deeply incised Sutlej Valley (Fig. 1). The Himalayan Crest region comprises the high mountain peaks of the Himalaya and leeward areas that are characterized by high relief, abundant snowfall, a

HESSD
9, 541–594, 2012

high degree of glaciation, and sparse vegetation. The Baspa, Wanger, and the southern part of the Spiti catchment belong to the Himalayan Crest region. High elevations, low relief and almost no vegetation due to arid climatic conditions characterize the Tibetan Plateau region, which comprises the northern part of the Spiti catchment and the Sutlej catchment upstream of Namgia (the so-called Zhada basin).

2.2 Climatic and geologic setting

Precipitation in the western Himalaya has pronounced seasonal and spatial variations (Bookhagen and Burbank, 2010). Most snowfall occurs between December and March and increases with elevation (Singh and Kumar, 1997; Wulf et al., 2010). From mid-July to mid-September the Indian monsoon accounts for intense rainfall, which is focused at elevations of 900 ± 400 m and 2100 ± 300 m a.s.l. at the southern Himalayan Front (Bookhagen and Burbank, 2006). The Higher Himalaya acts as an orographic barrier that inhibits most monsoonal moisture to migrate northward into the orogen and therefore creates a steep orographic rainfall gradient. Rainfall decreases from >2 m at the frontal parts to <0.2 m in the interior parts of the orogen over a horizontal distance of <100 km (Wulf et al., 2010). The highly seasonal precipitation results in peak river discharges and sediment flux during the summer season and orographic processes result in pronounced spatial differences in runoff magnitude.

The rocks in the study area can be subdivided into several contrasting units, which are bounded by major north-dipping tectonic fault systems that run parallel along strike the mountain belt (e.g. Burchfiel et al., 1992; Fuchs, 1975; Gansser, 1964; Heim and Gansser, 1939; Hodges, 2000). From southwest to northeast these units comprise (a) the Sub-Himalaya foreland basin, which contains detrital sediments derived from erosion of the orogen (Vannay et al., 2004); (b) the Lesser Himalaya Sequence (LHS), which mainly consists of massive quartz-arenites intruded by basalts (Miller et al., 2000); (c) the medium- to high-grade metamorphic sequence of the Lesser Himalayan Crystalline Sequence (LHCS), which consists of mylonitic micaschist, granitic gneiss with minor metabasite and quartzite (Vannay and Grasemann, 1998); (d) the

HESSD
9, 541–594, 2012

Higher Himalaya Crystalline Sequence (HHCS), which is composed of amphibolite facies to migmatitic paragneisses with minor metabasites, calc-silicate gneisses, and granitic gneisses often intruded by granitic plutons (Thiede et al., 2004, 2006; Vannay and Grasemann, 1998); and (e) the weakly metamorphosed sediments of the Tethyan Himalayan Sequence (THS), which consists of metapelites and metapsammites that comprise the cover sediments of the former Indian continental margin (e.g. Vannay et al., 2004).

The continuous northeastward movement of India with respect to Eurasia at a present rate of ca. 35 mm yr^{-1} (Larson et al., 1999; Wang et al., 2001) causes considerable seismic activity in the Himalaya (Bilham et al., 2001). During the past five decades, 20 earthquakes with magnitude ≥5 were recorded in the Sutlej Valley (Fig. 1a). Whereas large NW–SE shortening earthquakes at the Himalayan Front are related to the underthrusting of India beneath Eurasia, shallow (<15 km) earthquakes at the Himalayan Crest and Tibetan Plateau mainly document ongoing E–W extension (Hintersberger et al., 2010).

3 Data sets and methods

In the Indian part of the Sutlej Valley, several hydropower companies operate a dense network of weather stations and measure river discharge and suspended sediment concentrations (SSC). River discharge measurements are based on stage-discharge rating curves, which are annually recalculated during low-flow conditions in winter, because of channel bed changes. Year-round SSC sampling of the Sutlej River and several of its tributaries is done at the water surface and close to the riverbank. Given the high velocity and turbulence of the streams, we assume a high degree of sediment mixing and that the SSC samples are therefore representative of the entire water column.

In our analysis, river discharge and SSC data represent the daily average of usually two measurements, one in the early morning and one during late afternoon. In the

HESSD
9, 541–594, 2012

Baspa River and the Sutlej River at Wangtoo measurements are conducted on a 6-hourly and hourly basis, respectively. Despite the high sampling frequency of the Sutlej River at Wangtoo, we had only access to the daily minimum and maximum SSC data, of which we calculated the arithmetic mean for our analysis.

We use the measurements of daily river discharge, Q ($\mathrm{m^3\,s^{-1}}$), and suspended sediment concentration, SSC ($\mathrm{g\,l^{-1}}$), to calculate the suspended sediment load, SSL ($\mathrm{t\,yr^{-1}}$), and the suspended sediment yield, SSY ($\mathrm{t\,km^{-2}\,yr^{-1}}$), according to:

$$\mathrm{SSL} = \sum_{i=1}^{365} (Q(i) \cdot \mathrm{SSC}(i)) \tag{1}$$

$$\mathrm{SSY} = \mathrm{SSL}/A \tag{2}$$

where A is the catchment area ($\mathrm{km^2}$). We convert daily river discharge ($\mathrm{m^3\,s^{-1}}$) to part of the annual runoff, R ($\mathrm{m\,yr^{-1}}$), according to:

$$R = \frac{\sum_{i=1}^{365} Q(i)}{A}. \tag{3}$$

To investigate links between extreme events of suspended sediment flux and rainfall we use the TRMM product 3B42, which has a spatial resolution of $0.25^\circ \times 0.25^\circ$ (~30 km × 30 km) and a temporal resolution of 3 h. This data set combines microwave and infrared rain-rate estimates from sensors onboard several low-earth orbit and one geosynchronous satellite, which have been rescaled with monthly rain-gauge data (Huffman et al., 2007). The recently published APHRODITE rainfall dataset (Yatagai et al., 2009) has been shown to be a good rainfall indicator in the central Himalaya, where data density is high (Andermann et al., 2011). However, in the western Himalaya, rainfall stations are sparse, especially in the upper Sutlej area. Hence, we here rely on the satellite-derived rainfall data product TRMM 3B42.

HESSD
9, 541–594, 2012

We calculated the daily catchment-average TRMM rainfall for each catchment from 1998 to 2009 and define *rainstorms* as rainfall days exceeding the 90th percentile of all precipitation days $\geq 2\,\text{mm}\,\text{day}^{-1}$ during the 12-year catchment rainfall time series (Fig. 2). Rainfall in the 90th percentile has been previously associated with extreme rainfall events (e.g. Bookhagen, 2010; Cayan et al., 1999; Krishnamurthy et al., 2009). Based on the same approach, we define *peak SSC days* as days exceeding the 99th percentile of the catchment SSC time series. In case of several successive peak SSC days, we refer to *peak SSC events*, which encompass a variable length of 2–7 days in our data. Such peak SSC events are characterized by an abrupt increase in SSC followed by a gradual decrease. We refer to peak SSC events if we assume that successive peak SSC days are related to a single trigger mechanism.

To study the control of snow and glacial melt water runoff on sediment flux we further use daily fractional snow cover (FSC) observations that are derived from the MODIS instrument onboard the Terra and Aqua satellites of the NASA Earth Observation System (Hall et al., 1995, 2002). Comparison of MODIS snow products with ground-based snow measurements in the western US and Austria have yielded accuracies of 94–95 % (Klein and Barnett, 2003; Parajka and Blöschl, 2006). We reduced data gaps due to clouds by combining Terra and Aqua observations from the same day and we corrected for artifacts introduced by large viewing angles and other systematic errors with spline interpolation on the FSC time series (Dozier et al., 2008; Gafurov and Bárdossy, 2009). The smoothing splines are weighted based on the sensor zenith angle, which is provided in the MODIS surface reflectance product MOD09GA (Dozier et al., 2008). Finally, we filled all remaining data gaps by piecewise linear interpolation (Fritsch and Carlson, 1980).

In order to obtain information on spatial variations in rock strength, we estimated the rock compressive strength using a Schmidt hammer on fresh bedrock surfaces at steep cliff faces of road cuts (Katz et al., 2000). We conducted measurements in the Spiti, Sutlej, and Baspa catchment, which cover different rock types that are characteristic for the entire Sutlej Valley (Fig. 1b). Individual measurements returning

HESSD
9, 541–594, 2012

Schmidt hammer rebound values <10 SHR probably indicate fractured rock and were discarded (e.g. Craddock et al., 2007). At each site, 10 to 40 measurements were made at 20-cm intervals.

4 Results

4.1 Relationship between river discharge and suspended sediment concentration

River discharge and suspended sediment concentration (SSC) are both characterized by a pronounced seasonality (Fig. 2). During winter (November to April) SSC is generally below 0.5 g l^{-1} because river discharge is confined to low flow conditions, as most precipitation above 2000 m a.s.l. falls in form of snow. During summer (May to October) rainfall, snow- and glacial melt increase the river discharge, which results in increased stream power and enhanced transport capacity that elevates SSC typically above 0.5 g l^{-1}. Consequently, the summer season accounts for more than 80 % of the annual river discharge budget and more than 98 % of the annual SSL budget (Table 1).

To assess the spatial variability of river discharge and SSC we cross correlate all gauging sites (Table 2). Here, we find strong correlations ($r^2 > 0.8$) in river discharge among all stations in the Himalayan Crest and Tibetan Plateau regions, which indicates similar nivo-glacial runoff regimes, whereas the smallest, mostly rain-fed Ganvi tributary at the Himalayan Front exhibits the weakest correlation with all other stations. The overall lower coefficient of determination among all SSC gauging stations indicates a higher spatial variability in SSC and is most likely due to variable response times between small- and large-scale catchments. The pronounced correlation of neighboring stations along the Sutlej River (bold numbers in Table 2) underpins our confidence in the data.

In all catchments we find a strong positive correlation between daily river discharge and daily SSC (Fig. 3), i.e. the higher the river discharge the higher the sediment

Discussion Paper | Discussion Paper | Discussion Paper | Discussion Paper |

HESSD

9, 541–594, 2012

Climatic controls on suspended sediment flux in the Sutlej River Valley

H. Wulf et al.

concentration. This correlation suggests increasing mobilization of transiently stored sediment along the river as the river discharge increases. However, some days are characterized by extraordinary high SSC values that occasionally range 1–2 orders of magnitude above the seasonal average and therefore exhibit large residuals from the sediment-rating curve (Fig. 3). Such peak SSC days, which we define as days exceeding the 99th SSC percentile, occur predominantly during July and August, i.e. the peak of the Indian monsoon season, when river discharge is highest due to additional snow and glacial melts. Therefore, peak SSC days are generally associated with a high sediment load. However, some peak SSC days also occur in June or September; but due to the generally lower runoff, they leave only a low imprint on the overall sediment budget (Fig. 4).

4.2 Peak suspended sediment concentration events

Peak SSC days occur almost annually in most catchments and can be traced in many cases throughout the Sutlej River network (Fig. 4). During the observation period (2001–2009) we find that peak SSC days appear to be concurrent with rainstorms, a lake outburst flood, and extreme melt events. In contrast, none of the peak SSC days was related to an earthquake, which occurred with magnitudes up to $M_S = 6.6$ (cf. Table A1). Between 2005 and 2007 we identify three major rainstorms, lasting together 7 days, which can be traced by several gauging stations in the Sutlej catchment. Their widespread simultaneous occurrence indicates that rainstorms can affect large areas.

The sediment amount transported during peak SSC events varies considerably among all catchments ranging between 5 % and 62 % of the overall SSL budget. In the largest catchment area of the Sutlej River at Wangtoo, which integrates most tributary catchments, peak SSC events (99th percentile) contribute ~30 % to the total suspended sediment flux (Table 3). In all catchments leeward (northward) of the main orographic barrier the 90th SSC percentile accounts for more than 50 % of the total suspended sediment flux (Fig. 5).

HESSD
9, 541–594, 2012

The foregone analysis indicated that peak SSC events frequently coincide with rainstorms (Fig. 4). While many of these peak SSC events occur on the same day as rainstorms, delays of up to 1 or 2 days can be observed (Fig. 6). Because these delays exclusively occur in the largest catchments, we suspect that they are related to routing of the discharge from the source areas to the gauging stations. Rainstorms associated with peak SSC events typically last for 1–3 days (Wulf et al., 2010). Our longest and most complete SSC time series, covering five to six years, stem from the Wanger and Baspa rivers and the Sutlej River at Wangtoo, and indicate that 57–80 % of all peak SSC events are directly related to rainstorms (Table 3). Rainstorm-related peak SSC events occur almost on an annual basis in the semi-arid orogenic interior. At the Sutlej River at Wangtoo, they account for ~20 % of the total suspended sediment flux.

Whereas peak SSC events are generally associated with the most intense rainstorms between July and August, numerous rainstorms (>90th percentile) throughout the monsoon season leave no significant imprint on the SSC record (Fig. 7).

4.3 Spatial patterns in suspended sediment yields

In the following we investigate the large-scale patterns of mean annual sediment flux in the Sutlej River network. The mean annual suspended sediment concentration (SSC) decreases downstream along the Sutlej River from the Tibetan Plateau to the Himalayan Crest, followed by an increase towards the Himalayan Front (Fig. 8a). In contrast to the 8-fold decrease in mean annual SSC from the Tibetan Plateau to the Himalayan Crest, runoff increases by a factor of 20 (Table 1) and therefore, mean annual suspended sediment yields (SSY) (eq. 1) continuously increase (Fig. 8a). Despite the high SSC levels at the Tibetan Plateau, low runoff in this arid region results in a comparably low SSY (ca. 250 $\mathrm{t\,km^{-2}\,yr^{-1}}$). On the contrary, the Himalayan Crest is characterized by high runoff along with moderate SSC, which results in moderately high levels of mean annual SSY (ca. 1000 $\mathrm{t\,km^{-2}\,yr^{-1}}$). At the Himalayan Front sediment concentration and runoff are both high resulting in high SSY (ca. 1500 $\mathrm{t\,km^{-2}\,yr^{-1}}$).

HESSD
9, 541–594, 2012

4.4 Seasonal variations of suspended sediment flux

In most catchments we find a weakly pronounced anticlockwise hysteresis loop of mean monthly sediment flux shown in a characteristic example for the Sutlej River at Wangtoo (Fig. 9a). This anticlockwise hysteresis loop is most pronounced in the Wanger River (Fig. 9b) and indicates less suspended sediment transport on the rising limb of the hydrograph (May, June) compared to the falling limb (September, October) for a given discharge. For individual years, we find a pronounced anticlockwise hysteresis loop in the daily sediment flux during 2001, 2002, 2006, and 2007. During these years, the differences between lower SSC in May and June and higher SSC during September and October are most distinctive. For the remaining years these seasonal differences are less pronounced or do not exist. During July and August, when the monsoonal rainfall and glacial discharge peak in this region, variations in daily SSC and river discharge are very pronounced and no characteristic daily pattern is recognizable. The simplified mean monthly hysteresis loop of individual years, however, is on an annual basis strongly influence by the timing and magnitude of peak SSC events, which can alter the orientation and shape of the mean monthly hysteresis. We argue that a mean monthly hysteresis loop based on time series ≥5 years provides a more accurate representation of the seasonal sediment flux, because it is less affected by infrequent extreme events.

4.5 Rock strength measurements

Differences in rock strength can influence the erodibility of different rock units and therefore SSC levels in the different Sutlej tributaries that are characterized by contrasting rock units. Our rock compressive-strength measurements of the studied rock types range between 12 and 74 SHR (Schmidt hammer rebound values). Within each rock type strength measurements vary widely, such that the average standard deviation is 8.5 SHR. Despite such variability, the average rock strength indicates some principle differences between rock types. The quartzite in the Lesser Himalayan Sequence

HESSD
9, 541–594, 2012

Title Page
Abstract | Introduction
Conclusions | References
Tables | Figures
◀I | ▶I
◀ | ▶
Back | Close
Full Screen / Esc
Printer-friendly Version
Interactive Discussion

is characterized by the highest rock strength (60.0 ± 6.6 SHR), whereas the granitic gneisses in the Lesser Himalayan Crystalline Sequence and the High Himalayan Crystalline Sequence indicate significantly lower rock strengths (40.7 ± 9.3 SHR), similar to the granitic intrusion in the Tethyan Himalayan Sequence (39.4 ± 10.3 SHR). Somewhat surprisingly, metasedimentary rocks of the Tethyan Himalayan Sequence yield, on average, a high rock strength (51.0 ± 7.6 SHR), which slightly exceeds the rock strength measurements of the paragneisses in the High Himalayan Crystalline Sequence (47.1 ± 8.7 SHR) (Fig. 10).

5 Discussion

In our study we observe an overall increase in suspended sediment flux from the Tibetan Plateau to the Himalayan Front. This spatial pattern could reflect either process-based differences, differences in erodibility, or gradients in sediment availability. Large downstream differences in erosion processes are likely between the arid Tibetan Plateau, the snowfall dominated Himalayan Crest, and the rainfall dominated Himalayan Front. Catchment-wide differences in vegetation cover and rock types also suggest pronounced variations in erosion susceptibility. Furthermore, the supply of sediment that can be mobilized during extreme hydrometeorological events with high runoff contrasts sharply along the Sutlej River. In the following we discuss variations in sediment availability and sediment supply based on their climatic and geologic controls and compare spatial patterns of sediment flux in the Himalaya.

5.1 Monsoonal controls on suspended sediment flux

During our observation period (2001–2009) we identified monsoonal rainstorms (>90th percentile) as the dominant driving mechanism to deliver sediments to the steams across different climatic zones from the Himalayan Front to the Tibetan Plateau.

HESSD
9, 541–594, 2012

Previous studies emphasized the high rainstorm magnitudes and frequencies at the Himalayan Front, which contrast the more pronounced rainstorm magnitude variability in the orographically shielded Himalayan Crest and Tibetan Plateau regions (Craddock et al., 2007; Wulf et al., 2010). This observation is supported by our SSC measurements, which indicate frequent, low-magnitude SSC pulses during rainstorms at the Himalayan Front and less frequent but high-magnitude SSC pulses at the Himalayan Crest and Tibetan Plateau region.

During a field visit in September 2009 (cf. Fig. 6a), we witnessed an intense rainstorm event in the semi-arid region leeward of the main orographic barrier, which triggered widespread rockfalls, debris flows, and mudflows. Similar events were previously observed during a prolonged intense rainfall phase at the end of August 2002 (Bookhagen et al., 2005). The correlation between peak SSC events and rainstorms suggests that rainstorms frequently trigger landslides and enhance fluvial erosion due to increased river discharge. However, several rainstorms throughout the monsoon season leave no significant imprint on the SSC record (Fig. 7). This effect may be related to the variations in sediment availability, rainstorm intensity, or soil moisture thresholds as identified in other parts of the Himalaya (e.g. Dahal and Hasegawa, 2008; Gabet, 2004; Soja and Starkel, 2007).

The frequent occurrence of peak SSC events during rainstorms in July and August could also indicate that rainfall-induced runoff in glacial and periglacial areas represents an important sediment source (e.g. Collins and Hasnain, 1995; Haritashya et al., 2006; Singh et al., 2003). This argument is supported by studies of water and sediment discharge from the Gangotri and Dokriani Glacier, western Himalaya, which indicate that glacial sediment flux peaks during monsoonal rainstorms (Haritashya et al., 2006; Singh et al., 2003; Thayyen et al., 2007). In addition, we observe the most pronounced anticlockwise SSC-hysteresis loop in the glaciated Wanger catchment, which indicates an increase in SSC during the course of the monsoon season. Because late in the season the snowline is elevated and more glacial and periglacial ground is exposed, we suspect that these areas may act as source regions from where stored sediments

HESSD
9, 541–594, 2012

are evacuated. Furthermore, the coeval temperature increase results in a decline in the frozen and permafrost areas.

5.2 Extreme melt events

Besides the apparent relation between rainstorms and peak sediment flux, there are few peak SSC events, which cannot be related to monsoonal rainfall. Such an event occurred in June 2008 in the Spiti tributary during the absence of major earthquakes (Table A1) or rainstorms (Fig. 11a). Instead, the increase in SSC from early to mid June corresponds closely to an increase in air temperature. Despite heavy rainfall during mid and late June the SSC decreased, which again corresponds to decreases in air temperature (Fig. 11a). This correlation suggests that the suspended sediment flux during this event was induced by changes in temperature, which suggests a snow- or glacial-melt related source for the sediment discharge. During the initiation of this peak SSC event, snow coverage was less than 15 % in the Spiti catchment and decreased moderately during the peak sediment discharge from 14.2 to 8.8 % (Fig. 11b). Therefore, it is unlikely that snow avalanches or snow melt derived floods mobilized large amounts of sediment. In contrast, glacial ablation initiated, as the snowline retreated to glacial elevations, which generally corresponds to the evacuation of subglacial sediment (e.g. Haritashya et al., 2006). We suggest that sediments mobilized by glacial meltwaters most likely account for this peak SSC event. For the measurement period from 23 April to 29 August 2008 this suspended sediment discharge event (3–29 June) accounted for 58 % of the total suspended sediment flux, corresponding to 3.1 Mt of suspended sediment load.

In the western Himalaya, recent increases in surface temperatures caused the retreat of most glaciers (ca. 20–50 $\mathrm{m\,yr^{-1}}$) over the past decades (Bhambri and Bolch, 2009). As a result, these glaciers expose unstable paraglacial landscapes, which are highly susceptible to erosion processes driven by glacial runoff and rainfall (e.g. Meigs et al., 2006). Furthermore, the increase in surface temperatures increased the flood risk imposed by glacial lakes and caused widespread permafrost degradation, which

HESSD
9, 541–594, 2012

Title Page
Abstract | Introduction
Conclusions | References
Tables | Figures
◀◀ | ▶▶
◀ | ▶
Back | Close
Full Screen / Esc
Printer-friendly Version
Interactive Discussion

in turn decreases the slope stability and enhances erosion processes (Cheng and Wu, 2007; Lawrence and Slater, 2005; Zhao et al., 2004). Likewise, large areas in the western Himalaya experienced reduced snow-cover (Shekhar et al., 2010) as more precipitation falls in form of rain. Therefore, recent climate change enhances surface erosion processes, especially in the glacial and periglacial regions.

5.3 The 26 June 2005, Parechu Flood

Floods efficiently erode and transport sediment stored in the riverbed (Baker and Kale, 1998; Bookhagen et al., 2005; Coppus and Imeson, 2002; Hartshorn et al., 2002). On 26 June 2005 a flood occurred in the Parechu River, the main tributary of the Spiti River, which was caused by the failure of a landslide dam that blocked the river. The landslide occurred in late spring/early summer of 2004 and formed an artificial lake, which covered an area of 1.9 km^2 with a maximum depth of about 40 m storing about 64×10^6 m^3 of water in September 2004 (Gupta and Sah, 2007). The dam failure released a flood wave of about 20 m in height with a maximum discharge of about 2000 $m^3 s^{-1}$ estimated at the confluence with the Sutlej (Gupta and Sah, 2007). The 4-year averaged discharge at this site is 100 $m^3 s^{-1}$. Farther downstream the peak SSC of the Sutlej River at Wangtoo was measured to be 151 $g l^{-1}$ (SJVNL, 2005) with an estimated peak discharge of 4000 $m^3 s^{-1}$ (Kumar et al., 2007). The day preceding the flood, TRMM indicates heavy rainfall of 10–20 mm day^{-1} in semi-arid areas upstream of the landslide, which coincides with pronounced snow melt as indicated by MODIS imagery between 23 and 27 June 2005. During the 5-day period, snow cover in the upstream area (5294 km^2) reduced by 52.3 % from 830.1 km^2 (15.7 %) to 395.8 km^2 (7.5 %). Therefore, it is likely that the dam failure was triggered by a combination of rainfall and rain-on-snow event, which caused an increase in river discharge and hydrostatic pressure on the dam.

We estimate the suspended sediment load of the flood event (26 June–3 July 2005) at the Sutlej River at Wangtoo to be about 34 Mt, which equates to 88 $t km^{-2} day^{-1}$ or 41 % of the 2005 suspended sediment budget. This conservative estimate (likely an

Discussion Paper | Discussion Paper | Discussion Paper | Discussion Paper |

HESSD

9, 541–594, 2012

Climatic controls on suspended sediment flux in the Sutlej River Valley

H. Wulf et al.

underestimation) is based on an average daily discharge of 2000 $m^3 s^{-1}$ and a SSC of 50 $g l^{-1}$ for the flood day, for which only limited measurements are available (Fig. 6c). The estimated SSC of average daily of 50 $g l^{-1}$ is constrained by a maximum SSC of 151 $g l^{-1}$ on 26 June and a minimum SSC of 32 $g l^{-1}$ on 27 June. The decrease in SSC during the eight-day period after the flooding day was rather linear as compared to the exponential decrease during rainstorms (Fig. 6), which might be caused by the exceptionally high river discharge (~1700 $m^3 s^{-1}$) until 30 June 2005. Compared to the total eight peak SSC events measured at the Sutlej River at Wangtoo during 2004–2009 the Parechu Flood accounted for 51 % of the total suspended sediment load transported during these peak SSC events. Due to its prolonged duration (eight days) it was almost three times the magnitude of the highest rainfall induced peak SSC event (five day duration) in the same year (Fig. 6c). Therefore, the Parechu Flood can be considered as the dominant erosional event during our observation period (2001–2009).

5.4 Geologic controls on suspended sediment flux

The supply of sediment that can be mobilized during extreme events with high runoff contrasts sharply along the Sutlej River. In the Tibetan Plateau region many hillslopes feature large alluvial fans at their base, which provide abundant sediments that can be easily mobilized by increased river discharge or rainstorms (Fig. 12a). We argue that glacial and periglacial processes are highly efficient to erode these layered and densely fractured metasedimentary rocks (Heimsath and McGlynn, 2008; Molnar et al., 2007). The decrease in mean annual SSC from the Tibetan Plateau towards the Himalayan Crest is primarily caused by an increase in runoff through snow and glacial melt, which dilutes the suspended sediment concentration. This increase in runoff results in an increase in transport capacity, which also includes a higher bedload fraction (e.g. Pratt-Sitaula et al., 2007). In contrast to the bare Himalayan Crest and Tibetan Plateau, the Himalayan Front is characterized by lush vegetation, which indicates highly developed soils. Despite the protective vegetation cover, these soils are commonly detached by rain splash, surface runoff, creep, bioturbation, and shallow landsliding (Burbank, 2009; Morgan, 2004). In addition, large fluvial terraces and alluvial fans characterize the lower-elevation Sutlej River and tributaries (Bookhagen et al., 2006), because wider river valleys and lower river gradients allow larger storage volumes for sediments, which can be reworked during higher discharges (Fig. 12c). Because of this high sediment availability, which is mobilized by pronounced orographic rainfall, increased SSC characterizes the rivers of the Himalayan Front.

In order to characterize the erodibility of different rock types, we measured the rock compressive strength with a Schmidt hammer and identified rock-type specific variations. In comparison to rock strength measurements from the central Himalaya by Craddock et al. (2007), we find similar rock strength magnitudes in Lesser and High Himalaya. However, in the Tethyan Himalayan Sequence Craddock et al. (2007) observe a reduction in rock strength, which contrasts our finding of increased rock strength within the metasedimentary series. These differences may be explained by variable rock types, differences in grain size, and joint spacing gradients within in the Tethyan Himalayan Sequence (Aydin and Basu, 2005). In our study area the Tethyan metasedimentary sequence is characterized by a high joint density oriented along the foliation, which greatly reduces the rock cohesive strength (e.g. Selby, 1980). This low cohesive strength may result in a high erodibility, despite an overall high rock compressive strength indicated by the Schmidt hammer measurements. Therefore, our rock compressive strength measurements do not provide comprehensive insights on variation of rock type erodibility.

Our analysis suggests that low- and intermediate-magnitude earthquakes ($M_S < 6$) have a low impact on the suspended sediment flux. During the 6.4 (M_S) earthquake 1999 in Garwal Himalaya, Barnard et al. (2001) found that only one third of all 338 reactivated and induced landslides reached the rivers. Therefore, we assume that low- to intermediate-magnitude earthquakes mobilize material, which is rarely evacuated by the rivers.

HESSD
9, 541–594, 2012

5.5 Spatial patterns in modern Himalayan erosion

Finally, we attempt to place our results in the context of Himalaya-wide suspended sediment flux measurements. Despite difficulties in comparing different time spans of suspended sediment yields (SSY), the long-term (>5 years) mean of the SSY in Himalayan rivers indicates some first-order spatial patterns.

In general, the elevated, arid regions are characterized by low sediment yields, due to the low runoff. This pattern is evident in the upstream catchments of the Indus, Chenab, Sutlej and Marsyandi Rivers (Table A2). In a downstream direction, the sediment yield of these rivers increases gradually with runoff due to the high sediment flux of tributaries with higher rainfall-triggered hillslope erosion and a high glacial density, indicating high snowfall magnitudes and sporadic, intense monsoonal rainfall events. Consequently, the general north-to-south increase in Himalayan precipitation and runoff is also reflected in the sediment flux (Fig. 13).

Sediment flux measurements in proglacial streams exhibit large variations in their suspended sediment yields (Table 4), which might be related to differences in lithologies, topography, glacial debris cover, and seasonal precipitation (Scherler et al., 2011a,b). Whereas some glaciers in the western Karakorum and western Himalaya are characterized by peak suspended sediment yields exceeding those in monsoonal regions, others in the eastern Karakorum or central Himalaya exhibit low sediment yields and are comparable to sediment yields from the arid Tibetan Plateau (Fig. 13). Consequently, the glacial sediment yield exerts a large influence on the sediment flux characteristics of their downstream rivers. This is exemplified by the high sediment yield of the Hunza River (3373 $t\,km^{-2}\,yr^{-1}$) that is fed by the Batura glacier (6086 $t\,km^{-2}\,yr^{-1}$), which contrasts the relatively low sediment yield of the Shyok River (924 $t\,km^{-2}\,yr^{-1}$) that is fed by the Siachen glacier (707 $t\,km^{-2}\,yr^{-1}$) (Tables 4 and A2).

HESSD
9, 541–594, 2012

6 Conclusions

In this study, we provide a comprehensive analysis of spatiotemporal patterns in suspended sediment flux of the Sutlej River Valley in the western Himalaya. Our analysis is based on gauge measurements of river discharge and suspended sediment concentrations (SCC) of eight catchments in the Sutlej River Valley. Moreover, we combine these data with remotely sensed rainfall and snow-cover data to elucidate driving mechanisms for peak SSC (≥99th percentile) days and assess their impact on the suspended sediment budget. Finally, we discuss the spatiotemporal sediment flux pattern in the context of climatic and geologic controls on sediment availability and supply. Our data reveal three key conclusions:

First, peak erosional events (≥99th SSC percentile) account for ~30 % of the suspended sediment flux. These peak SSC events coincide frequently (57–80 %) with rainstorms, which trigger rockfalls, debris flows, and other mass movements especially in the semi-arid to arid interior of the orogen. Further trigger of peak SSC events are related to extreme melt events and a large lake outburst flood. For example, the Parechu Flood in June 2005 was the dominant erosional event (35 Mt SSL) and accounted for 41 % of the seasonal suspended sediment flux. The remote-sensing data preceding the flood document significant rainfall and snow melt, exacerbating the hydrologic pressure on the dam.

Second, we observe an increase of suspended sediment flux from the Tibetan Plateau to the Himalayan Front. From north to south along this profile, runoff increases 20-fold, SCC decreases 8-fold from the arid Tibetan plateau to the Himalayan Crest and increases again 3-fold southward to the humid, frontal regions. This sediment flux gradient suggests that modern erosion in the western Himalaya is most pronounced at frontal regions, which are characterized by intense monsoonal rainfall and highly developed soils.

Third, in all but one catchment we find an anticlockwise hysteresis loop, which indicates more suspended sediment transport during late summer than during the onset

HESSD
9, 541–594, 2012

Climatic controls on suspended sediment flux in the Sutlej River Valley

H. Wulf et al.

of the monsoonal season. We suggest that increases in temperature and their impact on permafrost regions and glacial discharge, which peaks in August, play a vital role in mobilizing transiently stored material. Transient sediments are stored in wide river valleys at the Himalayan Front and in the arid Tibetan Plateau region, whereas little sediment is stored in the steep river sections of the Himalayan Crest. In future climate change scenarios, including continuous glacial retreat, permafrost degradation, and more frequent monsoonal rainstorms across the Himalaya, we expect an increase in peak SSC events, which will decrease the water quality in the far downstream reaches, impacting agriculture, drinking-water and hydropower generation.

Acknowledgements. This research was funded by the German Science Foundation (DFG, GRK 1364). The data used in this study were acquired as part of the Tropical Rainfall Measuring Mission (TRMM) sponsored by the Japan National Space Development Agency (NASDA) and the NASA. B. B. was supported with grants from NASA (NNX08AG05G) and NSF (EAR 0819874). D. S. was supported by the German Federal Ministry of Education and Research (BMBF, PROGRESS) We thank S. Kumar, C. Kumar, V. Negi, H. Negi, K. Srinivasan, D. P. Goel, S. Pathak, D. Shukla, who provided suspended sediment concentration and river discharge records for us. We are grateful to Tashi Longpo, Swami Ray, and Bishan Lal for their enduring support during fieldwork.

References

Ali, K. F. and De Boer, D. H.: Spatial patterns and variation of suspended sediment yield in the upper Indus River basin, northern Pakistan, J. Hydrol., 334, 368–387, 2007.

Andermann, C., Bonnet, S., and Gloaguen, R.: Evaluation of precipitation data sets along the Himalayan front, Geochem. Geophy. Geosys., 12, Q07023, doi:10.1029/2011gc003513, 2011.

Aydin, A. and Basu, A.: The Schmidt hammer in rock material characterization, Eng. Geol., 81, 1–14, 2005.

Baker, V. R. and Kale, V. S.: The role of extreme events in shaping bedrock channels, in: In Rivers Over Rock: Fluvial Processes in Bedrock Channels, edited by: Tinkler, K. J. and Wohl, E. E., Geophysics Monogrograph Series, Washington, DC, 153–165, 1998.

HESSD

9, 541–594, 2012

Climatic controls on suspended sediment flux in the Sutlej River Valley

H. Wulf et al.

Barnard, P. L., Owen, L. A., Sharma, M. C., and Finkel, R. C.: Natural and human-induced landsliding in the Garhwal Himalaya of northern India Geomorphology, 40, 21–35, 2001.
Bhambri, R. and Bolch, T.: Glacier mapping: a review with special reference to the Indian Himalayas, Prog. Phys. Geogr., 33, 672–704, 2009.
Bhutiyani, M.: Sediment load characteristics of a proglacial stream of Siachen Glacier and the erosion rate in Nubra valley in the Karakoram Himalayas, India, J. Hydrol., 227, 84–92, 2000.
Bierman, P. R.: Using in situ produced cosmogenic isotopes to estimate rates of landscape evolution: A review from the geomorphic perspective, J. Geophys. Res.-Solid, 99, 13885–13896, 1994.
Bilham, R., Gaur, V. K., and Molnar, P.: Earthquakes – Himalayan seismic hazard, Science, 293, 1442–1444, doi:10.1126/science.1062584, 2001.
Bookhagen, B.: Appearance of extreme monsoonal rainfall events and their impact on erosion in the Himalaya, Geomatics, Nat. Hazards Risk, 1, 37–50, 2010.
Bookhagen, B. and Burbank, D. W.: Topography, relief, and TRMM-derived rainfall variations along the Himalaya, Geophys. Res. Lett., 33, L08405, doi:10.1029/2006GL026037, 2006.
Bookhagen, B. and Burbank, D. W.: Toward a complete Himalayan hydrological budget: Spatiotemporal distribution of snowmelt and rainfall and their impact on river discharge, J. Geophys. Res., 115, F03019, doi:10.1029/2009JF001426, 2010.
Bookhagen, B. and Strecker, M.: Spatiotemporal trends in erosion rates across a pronounced rainfall gradient: examples from the south-central Andes, Earth Planet. Sc. Lett., in review, 2012.
Bookhagen, B., Thiede, R. C., and Strecker, M. R.: Abnormal monsoon years and their control on erosion and sediment flux in the high, arid northwest Himalaya, Earth Planet. Sc. Lett., 231, 131–146, 2005.
Bookhagen, B., Fleitmann, D., Nishiizumi, K., Strecker, M. R., and Thiede, R. C.: Holocene monsoonal dynamics and fluvial terrace formation in the northwest Himalaya, India, Geology, 34, 601–604, 2006.
Burbank, D.: Mountain Uplift and Climate Change, in: Encyclopedia of Paleoclimatology and Ancient Environments, edited by: Gornitz, V., Springer, 596–606, 2009.
Burbank, D. W., Leland, J., Fielding, E., Anderson, R. S., Brozovic, N., Reid, M. R., and Duncan, C.: Bedrock incision, rock uplift and threshold hillslopes in the northwestern Himalayas, Nature, 379, 505–510, 1996.

Burchfiel, B. C., Chen, Z., Hodges, K. V., Liu, Y., and Royden, L. H.: The South Tibetan Detachment System, Himalayan orogen: extension contemporaneous with and parallel to shortening in a collisional mountain, Geol. Soc. Am. Spec. Pap., 269, 1–42, 1992.

Burg, J. P., Nievergelt, P., Oberli, F., Seward, D., Davy, P., and Maurin, J.: The Namche Barwa syntaxis: evidence for exhumation related to compressional crustal folding, J. Southeast Asian Earth Sci., 16, 239–252, 1998.

Cayan, D. R., Redmond, K. T., and Riddle, L. G.: ENSO and Hydrologic Extremes in the Western United States, J. Climate, 12, 2881–2893, 1999.

Chakrapani, G. J. and Saini, R. K.: Temporal and spatial variations in water discharge and sediment load in the Alaknanda and Bhagirathi Rivers in Himalaya, India, J. Asian Earth Sci., 35, 545–553, 2009.

Cheng, G. D. and Wu, T. H.: Responses of permafrost to climate change and their environmental significance, Qinghai-Tibet Plateau, J. Geophys. Res.-Earth, 112, 10, 2007.

Clift, P. D., Shimizu, N., Layne, G. D., Blusztajn, J. S., Gaedicke, C., Schluter, H. U., Clark, M. K., and Amjad, S.: Development of the Indus Fan and its significance for the erosional history of the Western Himalaya and Karakoram, Geol. Soc. Am. Bull., 113, 1039–1051, 2001.

Clift, P. D., Hodges, K. V., Heslop, D., Hannigan, R., van Long, H., and Calves, G.: Correlation of Himalayan exhumation rates and Asian monsoon intensity, Nat. Geosci., 1, 875–880, 2008.

Collins, D. N. and Hasnain, S. I.: Runoff and sediment transport from giacierized basins at the Himalayan scale, Effects of Scale on Interpretation and Management of Sediment and Water Quality, Proceedings of a Boulder Symposium, July 1995, IAHS Publ. no. 226, 17–25, 1995.

Coppus, R. and Imeson, A. C.: Extreme events controlling erosion and sediment transport in a semi-arid sub-andean valley, Earth Surf. Proc. Land., 27, 1365–1375, 2002.

Craddock, W. H., Burbank, D. W., Bookhagen, B., and Gabet, E. J.: Bedrock channel geometry along an orographic rainfall gradient in the upper Marsyandi River valley in central Nepal, J. Geophys. Res.-Earth, 112, F03007, doi:10.1029/2006JF000589, 2007.

Curray, J. R., Emmel, F. J., and Moore, D. G.: The Bengal Fan: morphology, geometry, stratigraphy, history and processes, Mar. Petrol. Geol., 19, 1191–1223, 2003.

Dahal, R. K. and Hasegawa, S.: Representative rainfall thresholds for landslides in the Nepal Himalaya, Geomorphology, 100, 429–443, 2008.

Dozier, J., Painter, T. H., Rittger, K., and Frew, J. E.: Time-space continuity of daily maps of fractional snow cover and albedo from MODIS, Adv. Water Resour., 31, 1515–1526, 2008.

Finlayson, D. P., Montgomery, D. R., and Hallet, B.: Spatial coincidence of rapid inferred erosion within young metamorphic massifs in the Himalayas, Geology, 30, 219–222, 2002.
Finnegan, N. J., Hallet, B., Montgomery, D. R., Zeitler, P. K., Stone, J. O., Anders, A. M., and Yuping, L.: Coupling of rock uplift and river incision in the Namche Barwa-Gyala Peri massif, Tibet, Geol. Soc. Am. Bull., 120, 142–155, 2008.
Fritsch, F. N. and Carlson, R. E.: Monotone Piecewise Cubic Interpolation, SIAM J. Numer. Anal., 7, 238–246, 1980.
Fuchs, G.: Contributions to the geology of the North-Western Himalayas, Abhandlungen der Geologischen Bundesanstalt, Vienna, 32, 59, 1975.
Gabet, E.: Rainfall thresholds for landsliding in the Himalayas of Nepal, Geomorphology, 63, 131–143, 2004.
Gabet, E. J., Burbank, D. W., Pratt-Sitaula, B., Putkonen, J., and Bookhagen, B.: Modern erosion rates in the High Himalayas of Nepal, Earth Planet. Sc. Lett., 267, 482–494, 2008.
Gafurov, A. and Bárdossy, A.: Cloud removal methodology from MODIS snow cover product, Hydrol. Earth Syst. Sci., 13, 1361–1373, doi:10.5194/hess-13-1361-2009, 2009.
Galy, A. and France-Lanord, C.: Higher erosion rates in the Himalaya: Geochemical constraints on riverine fluxes, Geology, 29, 23–26, 2001.
Gansser, A.: The Geology of the Himalayas, Wiley Interscience, New York, 1964.
Gardner, J. S. and Jones, N. K.: Sediment transport and yield in the Raikot glacier, in: Himalaya to the Sea: Geology, Geomorphology and the Quaternary, edited by: Shroder, J. F. and Shroder, J. F. J., Routledge, 2002.
Gupta, V. and Sah, M. P.: Impact of the Trans-Himalayan Landslide Lake Outburst Flood (LLOF) in the Satluj catchment, Himachal Pradesh, India, Nat. Hazards, 45, 379–390, 2007.
Hall, D., Riggs, G. A., Salomonson, V. V., DiGirolamo, N. E., and Bayr, K. J.: MODIS snow-cover products, Remote Sens. Environ., 83, 181–194, 2002.
Hall, D. K., Riggs, G. A., and Salomonson, V. V.: Development of Methods for Mapping Global Snow Cover Using Moderate Resolution Imaging Spectroradiometer Data, Remote Sens. Environ., 54, 127–140, 1995.
Haritashya, U. K., Singh, P., Kumar, N., and Gupta, R. P.: Suspended sediment from the Gangotri Glacier: Quantification, variability and associations with discharge and air temperature, J. Hydrol., 321, 116–130, 2006.
Hartshorn, K., Hovius, N., Dade, W. B., and Slingerland, R. L.: Climate-driven bedrock incision in an active mountain belt, Science, 297, 2036–2038, 2002.

HESSD
9, 541–594, 2012

Heim, A. and Gansser, A.: Central Himalaya Geological Observations of the Swiss Expedition 1936, Zurich, 246, 1939.
Heimsath, A. M. and McGlynn, R.: Quantifying periglacial erosion in the Nepal high Himalaya, Geomorphology, 97, 5–23, 2008.
Henck, A. C., Montgomery, D. R., Huntington, K. W., and Liang, C. A.: Monsoon control of effective discharge, Yunnan and Tibet, Geology, 38, 975–978, doi:10.1130/g31444.1, 2010.
Hintersberger, E., Thiede, R., Strecker, M., and Hacker, B.: East-west extension in the NW Indian Himalaya, Geol. Soc. Am. Bull., 122, 1499–1515, 2010.
Hodges, K. V.: Tectonics of the Himalaya and southern Tibet from two perspectives, Geol. Soc. Am., Bull., 112, 324–350, 2000.
Hodges, K. V., Wobus, C., Ruhl, K., Schildgen, T., and Whipple, K.: Quaternary deformation, river steepening, and heavy precipitation at the front of the Higher Himalayan ranges, Earth Planet. Sc. Lett., 220, 379–389, 2004.
Huete, A., Didan, K., Miura, T., Rodriguez, E. P., Gao, X., and Ferreira, L. G.: Overview of the radiometric and biophysical performance of the MODIS vegetation indices, Remote Sens. Environ., 83, 195–213, 2002.
Huffman, G. J., Adler, R. F., Bolvin, D. T., Gu, G., Nelkin, E. J., Bowman, K. P., Hong, Y., Stocker, E. F., and Wolff, D. B.: The TRMM Multisatellite Precipitation Analysis (TMPA): Quasi-Global, Multiyear, Combined-Sensor Precipitation Estimates at Fine Scales, J. Hydrometeorol., 8, 33–55, 2007.
IPCC: IPCC Fourth Assessment Report: Working Group II Report “Impacts, Adaptation and Vulnerability”, Fourth Assessment Reportof the Intergovernmental Panel on Climate Change, edited by: Parry, M. L., Canziani, O. F., Palutikof, J. P., van der Linden, P. J., and Hanson, C. E., Cambridge University Press, 2007.
Jain, S. K., Singh, P., Saraf, A. K., and Seth, S. M.: Estimation of sediment yield for a rain, snow and glacier fed river in the Western Himalayan region, Water Resour. Manage., 17, 377–393, 2003.
Jha, P. K., Subramanian, V., and Sitasawad, R.: Chemical and sediment mass transfer in the Yamuna River – A tributary of the Ganges system, J. Hydrol., 104, 237–246 1988.
Katz, O., Reches, Z., and Roegiers, J.-C.: Evaluation of mechanical rock properties using a Schmidt Hammer, Int. J. Rock Mech. Min. Sci., 37, 723–728, 2000.

HESSD
9, 541–594, 2012

Kirchner, J. W., Finkel, R. C., Riebe, C. S., Granger, D. E., Clayton, J. L., King, J. G., and Megahan, W. F.: Mountain erosion over 10 yr, 10 k.y., and 10 m.y. time scales, Geology, 29, 591–594, 2001.

Klein, A. G. and Barnett, A. C.: Validation of daily MODIS snow cover maps of the Upper Rio Grande River Basin for the 2000–2001 snow year, Remote Sens. Environ., 86, 162–176, 2003.

Krishnamurthy, C. K. B., Lall, U., and Kwon, H.-H.: Changing Frequency and Intensity of Rainfall Extremes over India from 1951 to 2003, J. Climate, 22, 4737–4746, 2009.

Kumar, R., Bales, J. D., Jubach, R., Gyamba, P. D., Kane, M. D., and Scott, A. C.: Flash-Flood Warning for the Upper Sutlej River Basin, Northern India, http://cedb.asce.org/cgi/WWWdisplay.cgi?165529 (last access: January 2012), 2007.

Lal, D., Harris, N. B. W., Sharma, K. K., Gu, Z., Ding, L., Liu, T., Dong, W., Caffee, M. W., and Jull, A. J. T.: Erosion history of the Tibetan Plateau since the last interglacial: constraints from the first studies of cosmogenic 10Be from Tibetan bedrock, Earth Planet. Sc. Lett., 217, 33–42, 2003.

Larson, K., Buergmann, R., Bilham, R., and Freymueller, J. T.: Kinematics of the India-Eurasia collision zone from GPS measurements, J. Geophys. Res., 104, 1077–1093, 1999.

Lawrence, D. M. and Slater, A. G.: A projection of severe near-surface permafrost degradation during the 21st century, Geophys. Res. Lett., 32, 5, 2005.

Meade, R. H.: Movement and storage of sediment in river systems, in: Physical and chemical weathering in geochemical cycles, edited by: Lerman, A. and Meybeek, M., Kluver, Dordrecht, 165–179, 1988.

Meigs, A., Krugh, W. C., Davis, K., and Bank, G.: Ultra-rapid landscape response and sediment yield following glacier retreat, Icy Bay, southern Alaska, Geomorphology, 78, 207–221, doi:10.1016/j.geomorph.2006.01.029, 2006.

Miller, C., Kloetzli, U., Frank, W., Thoeni, M., and Grasemann, B.: Proterozoic crustal evolution in the NW Himalaya (India) as recorded by circa 1.80 Ga mafic and 1.84 Ga granitic magmatism, Precambrian Res., 103, 191–206, 2000.

Milliman, J. D. and Syvitski, J. P. M.: Geomorphic/Tectonic Control of Sediment Discharge to the Ocean: The Importance of Small Mountainous Rivers, J. Geol., 100, 525–544, 1992.

Molnar, P. and England, P.: Late Cenozoic uplift of mountain ranges and global climate change: chicken or egg?, Nature, 346, 29–34, 1990.

HESSD

9, 541–594, 2012

Climatic controls on suspended sediment flux in the Sutlej River Valley

H. Wulf et al.

Molnar, P., Anderson, R. S., and Anderson, S. P.: Tectonics, fracturing of rock, and erosion, J. Geophys. Res., 112, 1–12, 2007.
Morgan, R. P. C.: Soil erosion and conservation, Wiley-Blackwell, 320 pp., 2004.
Ohta, T., Fukushima, Y., Suzuki, M., Motoyama, H., Kawashima, K., and Kubota, H.: Suspended sediment yield in a glaciated watershed of Langtang valley, Nepal Himalayas, Bull. Glacier Res., 5, 19–24, 1987.
Parajka, J. and Blöschl, G.: Validation of MODIS snow cover images over Austria, Hydrol. Earth Syst. Sci., 10, 679–689, doi:10.5194/hess-10-679-2006, 2006.
Pratt-Sitaula, B., Garde, M., Burbank, D. W., Oskin, M., Heimsath, A., and Gabet, E.: Bedload-to-suspended load ratio and rapid bedrock incision from Himalayan landslide-dam lake record, Quaternary Res., 68, 111–120, 2007.
Puri, V. M. K.: Glaciohydrological and suspended sediment load studies in the melt water channel of Changme Khangpu Glacier, Mangam district, Sikkim, Symposium on Snow, Ice and Glaciers – Himalayan Prospective, Lucknow, 1999.
Rao, S. V. N., Rao, M. V., and Ramasasitri, K. S.: A Study of Sedimentation in Chenab Basin in Western Himalayas, Nord. Hydrol., 28, 201–216, 1997.
Raymo, M. E., Ruddiman, W. E., and Froelich, P. N.: Influence of late Cenozoic mountain building on ocean geochemical cycles, Geology, 16, 649–653, 1988.
Raymo, M. E. and Ruddiman, W. F.: Tectonic forcing of late Cenozoic climate, Nature, 359, 117–122, 1992.
Reiners, P. W., Ehlers, T. A., and Zeitler, P. K.: Past, Present, and Future of Thermochronology, Rev. Mineral. Geochem., 58, 1–18, 2005.
Scherler, D., Bookhagen, B., and Strecker, M. R.: Hillslope-glacier coupling: the interplay of topography and glacial dynamics in High Asia, J. Geophys. Res., 116, 21 pp., doi:10.1029/2010JF001751, 2011a.
Scherler, D., Bookhagen, B., and Strecker, M. R.: Spatially variable response of Himalayan glaciers to climate change affected by debris cover, Nat. Geosci., 4, 156–159, doi:10.1038/ngeo1068, 2011b.
Selby, M. J.: A rock mass strength classification for geomorphic purposes: with tests from Antarctica and New Zealand, Z. Geomorphol., 24, 31–51, 1980.
Shekhar, M. S., Chand, H., Kumar, S., Srinivasan, K., and Ganju, A.: Climate-change studies in the western Himalaya, Ann. Glaciol., 51, 105–112, 2010.

HESSD
9, 541–594, 2012

Singh, P. and Kumar, N.: Effect of orography on precipitation in the western Himalayan region, J. Hydrol., 199, 183–206, 1997.
Singh, P., Ramasatri, K. S., Kumar, N., and Bhatnagar, N. K.: Suspended Sediment Transport from the Dokriani Glacier in the Garhwal Himalayas, Nord. Hydrol., 34, 221–244, 2003.
Sinha, R. and Friend, P. F.: River systems and their sediment flux, Indo-Gangetic plains, Northern Bihar, India, Sedimentology, 41, 825–845, 1994.
SJVNL: Concept paper on silt content in Satluj river, Satluj Jal Vidyut Nigam Limited, Satluj Jal Vidyut Nigam Limited, Shimla, India, 2005.
Small, E. E. and Anderson, R. S.: Geomorphically driven late Cenozoic rock uplift in the Sierra Nevada, California, Science, 270, 277–280, 1995.
Soja, R. and Starkel, L.: Extreme rainfalls in Eastern Himalaya and southern slope of Meghalaya Plateau and their geomorphologic impacts, Geomorphology, 84, 170–180, 2007.
Stewart, R. J., Hallet, B., Zeitler, P. K., Malloy, M. A., Allen, C. M., and Trippett, D.: Brahmaputra sediment flux dominated by highly localized rapid erosion from the easternmost Himalaya, Geology, 36, 711–714, 2008.
Thayyen, R. J., Gergan, J. T., and Dobhal, D. P.: Role of glaciers and snow cover on headwater river hydrology in monsoon regime – Micro-scale study of Din Gad catchment, Garhwal Himalaya, India, Current Sci., 92, 376–382, 2007.
Thiede, R. C., Bookhagen, B., Arrowsmith, J. R., Sobel, E. R., and Strecker, M. R.: Climatic control on rapid exhumation along the Southern Himalayan Front, Earth Planet. Sc. Lett., 222, 791–806, 2004.
Thiede, R. C., Arrowsmith, J. R., Bookhagen, B., McWilliams, M., Sobel, E. R., and Strecker, M. R.: Dome formation and extension in the Tethyan Himalaya, Leo Pargil, northwest India, Bull. Geol. Soc. Am., 118, 635–650, 2006.
Thiede, R. C., Ehlers, T. A., Bookhagen, B., and Strecker, M. R.: Erosional variability along the northwest Himalaya, J. Geophys. Res., 114, F01015, doi:10.1029/2008JF001010, 2009.
Vance, D., Bickle, M., Ivy-Ochs, S., and Kubik, P. W.: Erosion and exhumation in the Himalaya from cosmogenic isotope inventories of river sediments, Earth Planet. Sc. Lett., 206, 273–288, 2003.
Vannay, J.-C. and Grasemann, B.: Inverted metamorphism in the High Himalaya of Himachal Pradesh (NW India): Phase equilibria versus thermobarometry, Schweiz, Mineral. Petrogr. Mitt., 78, 107–132, 1998.

Vannay, J. C., Grasemann, B., Rahn, M., Frank, W., Carter, A., Baudraz, V., and Cosca, M.: Miocene to Holocene exhumation of metamorphic crustal wedges in the NW Himalaya: Evidence for tectonic extrusion coupled to fluvial erosion, Tectonics, 23, 1–24, 2004.

von Blanckenburg, F.: The control mechanisms of erosion and weathering at basin scale from cosmogenic nuclides in river sediment, Earth Planet. Sc. Lett., 237, 462–479, 2005.

Wang, Q., Zhang, P.-Z., Freymueller, J. T., Bilham, R., Larson, K. M., Lai, X. A., You, X., Niu, Z., Wu, J., Li, Y., Liu, J., Yang, Z., and Chen, Q.: Present-Day Crustal Deformation in China Constrained by Global Positioning System Measurements, Science, 294, 574–577, doi:10.1126/science.1063647, 2001.

Webb, A. A. G., Yin, A., Harrison, T. M., Celerier, J., Gehrels, G. E., Manning, C. E., and Grove, M.: Cenozoic tectonic history of the Himachal Himalaya (northwestern India) and its constraints on the formation mechanism of the Himalayan orogen, Geosphere, 7, 1013–1061, doi:10.1130/ges00627.1, 2011.

Wobus, C., Heimsath, A., Whipple, K., and Hodges, K.: Active out-of-sequence thrust faulting in the central Nepalese Himalaya, Nature, 434, 1008–1011, 2005.

Wolman, M. G. and Miller, J. P.: Magnitude and frequency of forces in geomorphic processes, J. Geol., 68, 54–74, 1960.

Wulf, H., Bookhagen, B., and Scherler, D.: Seasonal precipitation gradients and their impact on fluvial sediment flux in the Northwest Himalaya, Geomorphology, 118, 13–21, doi:10.1016/J.Geomorph.2009.12.003, 2010.

Yatagai, A., Arakawa, O., Kamiguchi, K., Kawamoto, H., Nodzu, M. I., and Hamada, A.: A 44-Year Daily Gridded Precipitation Dataset for Asia Based on a Dense Network of Rain Gauges, SOLA, 5, 137–140, 2009.

Zeitler, P. K., Melzer, A. S., Koons, P. O., Craw, D., Hallet, B., Chamberlain, C. P., Kidd, W. S. F., Park, S. K., Seeber, L., Bishop, M. P., and Shroder, J. F.: Erosion, Himalayan tectonics and the geomorphology of metamorphism, GSA Today, 11, 4–8, 2001.

Zhao, L., Ping, C. L., Yang, D. Q., Cheng, G. D., Ding, Y. J., and Liu, S. Y.: Changes of climate and seasonally frozen ground over the past 30 years in Qinghai-Xizang (Tibetan) Plateau, China, Global Planet. Change, 43, 19–31, 2004.

HESSD
9, 541–594, 2012

Climatic controls on suspended sediment flux in the Sutlej River Valley

H. Wulf et al.

Table 1. Topographic, climatic and hydrological characteristics of the studied watersheds. Locations of the catchments are indicated in Fig. 1. Summer indicates the period from May to October. The suspended sediment concentration (SSC) represents the annual mean.

Catchments	Topography				Climate				Hydrology			
	Area	Elevation		Relief	Ice	Snow	Rain	Vege-	Runoff		SSC	SSY
		min	max	(km/	area	area	TRMM	tation	summer		mean	($t\,km^{-2}$
	(km^2)	(km)	(km)	5 km)	(%)	(%)	($m\,yr^{-1}$)	NDVI	($m\,yr^{-1}$)	(%)	($g\,l^{-1}$)	yr^{-1})
Tributaries												
Ganvi	117	1.6	5.6	2.58	3.7	25.8	1.12	0.39	1.27	78.3	0.93	1507
Wanger	264	2.5	5.7	2.24	17.2	54.1	0.74	0.11	1.67	85.4	0.29	614
Baspa	989	2.5	6.4	2.21	24.0	54.0	0.93	0.09	1.14	89.5	0.80	1717
Spiti	12 477	2.6	6.7	1.68	6.7	37.4	0.36	0.03	0.26	86.9	1.45	499
Sutlej River												
at Namgia	30 950	2.6	7.2	0.93	1.8	19.8	0.38	0.08	0.06	85.1	2.59	223
at Jangi	44 738	2.2	7.2	1.21	3.6	25.6	0.39	0.07	0.13	81.5	1.85	302
at Karchham	46 291	1.9	7.2	1.22	3.6	25.7	0.39	0.07	0.16	85.3	2.37	556
at Wangtoo	48 316	1.5	7.2	1.27	4.1	26.5	0.41	0.07	0.20	85.9	2.20	615

Table 2. Correlation of daily river discharge (top) and daily suspended sediment concentration (bottom) among different gauging sites. Neighboring stations along the Sutlej, which are expected to correlate strongly, are marked bold.

River discharge (coefficient of determination)	Ganvi	Wanger	Baspa	Spiti	Sutlej at Namgia	Sutlej at Jangi	Sutlej at Karchham	Sutlej at Wangtoo
Ganvi	1	0.57	0.75	0.77	0.77	0.62	0.60	0.79
Wanger	–	1	0.91	0.84	0.86	0.95	0.84	0.92
Baspa	–	–	1	0.91	0.85	0.95	0.93	0.96
Spiti	–	–	–	1	0.81	0.95	0.91	0.92
Sutlej (Namgia)	–	–	–	–	1	**0.95**	0.93	0.91
Sutlej (Jangi)	–	–	–	–	–	1	**0.98**	0.98
Sutlej (Karchham)	–	–	–	–	–	–	1	**0.97**
Sutlej (Wangtoo)	–	–	–	–	–	–	–	1
Suspended sediment conc.	**Ganvi**	**Wanger**	**Baspa**	**Spiti**	**Sutlej at Namgia**	**Sutlej at Jangi**	**Sutlej at Karchham**	**Sutlej at Wangtoo**
Ganvi	1	0.43	0.17	0.32	0.08	0.38	−0.13	0.15
Wanger	–	1	0.31	0.56	0.49	–	0.80	0.41
Baspa	–	–	1	0.49	0.41	0.59	0.37	0.51
Spiti	–	–	–	1	0.64	0.92	0.66	0.82
Sutlej (Namgia)	–	–	–	–	1	**0.89**	0.73	0.87
Sutlej (Jangi)	–	–	–	–	–	1	**0.79**	0.82
Sutlej (Karchham)	–	–	–	–	–	–	1	**0.78**
Sutlej (Wangtoo)	–	–	–	–	–	–	–	1

HESSD
9, 541–594, 2012

Table 3. Peak suspended sediment concentration (SSC) event and their relation to rainstorms (>90th percentile), the *Parechu Flood*, and meltwaters. Peak SSC events combine successive peak SSC days (99th SSC percentile). Dashes indicate that no records were obtained during the Parechu Flood. Note the variable length of the records.

River	SSC record length	99th SSC percentile threshold	90th rainfall percentile threshold	Peak SSC events	Percent of SSL budget	Events caused by rainstroms		Event caused by the Parechu Flood		Events caused by meltwaters		Events with unknown trigger	
	(days)	($g\,l^{-1}$)	($mm\,day^{-1}$)	(#)	(%)	(#)	(%)	(#)	(%)	(#)	(%)	(#)	(%)
Tributaries													
Ganvi	215	5.5	19.2	1	5.6	1	100	0	0	0	0	0	0
Wanger	1470	1.3	18.0	5	9.8	4	80	0	0	0	0	1	20
Baspa	1867	2.1	18.5	7	61.9	4	57	0	0	1	14	2	29
Spiti	615	8.1	15.5	2	15.3	1	50	–	–	1	50	0	0
Sutlej River													
at Namgia	711	19.2	14.0	3	32.0	2	67	–	–	0	0	1	33
at Jangi	286	7.8	14.5	1	17.5	1	100	–	–	0	0	0	0
at Karchham	379	11.7	15.2	3	8.6	1	33	1	33	0	0	1	33
at Wangtoo	2059	14.4	15.4	8	30.1	6	75	1	13	0	0	1	13

HESSD
9, 541–594, 2012

Table 4. Suspended sediment flux in proglacial streams of the Himalaya and Karakorum. The catchment denudation rate is based on a bulk rock density of 2.65 g cm^{-3}, accounts only for the suspended sediment flux, and refers to the glacial catchment area, which exceeds the glacial area.

Glacier	River	Latitude [°]	Longitude [°]	Elevation [m]	Glacial area [km^2]	Obs. period	Runoff [m yr^{-1}]	Suspended-Sediment Load [10^6 t yr^{-1}]	Suspended-Sediment Yield [t km^{-2} yr^{-1}]	Catchment denudation [mm yr^{-1}]	Reference
Siachen	Nubra	35.11	77.23	3570	620.0	1987–1991	1.36	1.26	707	0.27	Bhutiyani (1999)
Batura	Hunza	36.49	74.89	2530	389.4	1990	1.93	3.95	6086	2.30	Collins (1995)
Raikot	Astore	35.38	74.59	3010	56.0	1986	1.01	0.32–0.49	3500–5250	1.3–2.0	Gardner and Jones (2002)
Gangotri	Bhagirathi	30.95	79.04	3830	286.0	2000–2003	0.99	2.69	4834	1.82	Haritashya et al. (2006)
Dokriani	Bhagirathi	30.86	78.78	3710	9.7	1995–1998	1.60	0.04	2700	1.02	Singh et al. (2003)
Langtang	Trisuli	28.23	85.69	4324	127.2	1985–1986	1.35	0.08	245	0.09	Ohta et al. (1987)
Changme	Tista	27.91	88.70	4650	4.5	–	–	0.003	668	0.25	Puri et al. (1999)

HESSD
9, 541–594, 2012

Table A1. List of earthquakes in the study area. Data provided by the Incorporated Research Institutions for Seismology (http://www.iris.washington.edu). Abbreviations of the magnitude types indicate the moment magnitude (MW), body-wave magnitude (MB), and surface-wave magnitude (MS). Abbreviations of the earthquake catalogues indicate the Bulletin of the International Seismological Centre (ISCCD), Quick Epicenter Determinations (QED), Monthly Hypocenter Data File (MHDF), Weekly Hypocenter Data File (WHDF), a list distributed by the National Earthquake Information Service (FINGER), and historical earthquake data listed in a hydropower project report (www.powermin.nic.in/whats_new/PFR/HP/Luhri_Hep.pdf).

Date	Time	Latitude	Longitude	Depth	Magnitude	Type	Catalog
4 Apr 2011	11:31:40	29.68	80.75	12.5	5.4	M	FINGER/NEIC
6 Jul 2010	19:08:26	29.84	80.40	32.8	5.2	MB	WHDF/NEIC
22 Jun 2010	23:14:11	29.87	80.43	16.3	5.2	MB	WHDF/NEIC
28 May 2010	07:25:03	31.14	77.84	18.8	5.0	MB	WHDF/NEIC
18 Mar 2010	07:52:29	34.33	81.76	37.2	5.0	MB	WHDF/NEIC
15 Mar 2010	20:17:17	30.53	81.88	17.8	5.0	MB	WHDF/NEIC
20 Nov 2009	07:16:59	30.76	83.45	19.0	5.1	MB	MHDF/NEIC
29 Sep 2009	06:01:13	30.89	83.49	10.0	5.0	MB	MHDF/NEIC
21 Sep 2009	09:43:51	30.88	79.06	52.3	5.0	MB	MHDF/NEIC
4 Jun 2009	02:54:48	32.78	81.76	7.2	5.2	MB	MHDF/NEIC
1 Apr 2009	02:34:37	33.66	82.44	10.0	5.0	MW	MHDF/NEIC
18 Feb 2009	10:11:44	30.67	83.86	35.0	5.1	MW	MHDF/NEIC
8 Dec 2008	08:59:09	29.99	82.09	15.3	5.3	MB	ISCCD/ISC
25 Sep 2008	01:47:12	30.84	83.59	10.0	5.4	MB	ISCCD/ISC
25 Aug 2008	14:16:03	30.82	83.56	7.6	5.1	MB	ISCCD/ISC
25 Aug 2008	13:39:39	30.93	83.46	10.0	5.1	MB	ISCCD/ISC
25 Aug 2008	13:22:02	31.06	83.65	25.5	6.6	MS	ISCCD/ISC
5 May 2007	08:51:40	34.27	82.03	14.2	5.7	MB	ISCCD/ISC
14 Dec 2005	07:09:52	30.51	79.25	36.9	5.4	ML	ISCCD/ISC
8 Apr 2005	19:51:42	30.48	83.62	60.0	5.0	MB	QED/NEIC
7 Apr 2005	20:04:40	30.52	83.66	14.7	6.1	MS	ISCCD/ISC
26 Oct 2004	02:11:31	31.04	81.08	4.0	5.9	MB	ISCCD/ISC
28 Jul 2004	22:22:18	30.64	83.60	51.0	5.1	MB	QED/NEIC
11 Jul 2004	23:08:42	30.72	83.67	8.1	6.2	MS	ISCCD/ISC

HESSD
9, 541–594, 2012

Table A1. Continued.

Date	Time	Latitude	Longitude	Depth	Magnitude	Type	Catalog
4 Jun 2002	14:36:03	30.57	81.42	10.0	5.4	MB	ISCCD/ISC
27 Nov 2001	17:56:57	29.55	81.75	42.7	5.0	MB	ISCCD/ISC
27 Nov 2001	08:53:54	29.55	81.75	33.0	5.3	MS	MHDF/NEIC
27 Nov 2001	07:31:52	29.61	81.75	33.0	5.6	MB	MHDF/NEIC
17 Jun 2000	16:34:13	32.00	78.41	38.8	5.6	MS	ISCCD/ISC
6 Apr 1999	19:37:24	30.48	79.56	16.5	5.5	MB	ISCCD/NDI
28 Mar 1999	19:36:09	30.31	79.36	36.3	6.1	MS	ISCCD/ISC
28 Mar 1999	19:05:12	30.51	79.42	22.9	6.4	MB	ISCCD/ISC
28 Mar 1999	19:04:50	30.72	75.13	33.0	5.9	MB	ISCCD/DJA
5 Jan 1997	08:47:25	29.87	80.56	24.9	5.3	MS	ISCCD/ISC
20 Oct 1993	16:15:59	28.69	82.25	–	5.1	MB	ISCCD/ISC
15 Sep 1993	15:08:15	33.33	75.74	43.7	5.0	MB	ISCCD/ISC
9 Dec 1991	01:02:42	29.51	81.61	2.9	5.6	MB	ISCCD/ISC
19 Oct 1991	21:23:15	30.77	78.79	13.2	6,4	MB	ISCCD/ISC
21 Sep 1990	16:08:19	29.98	79.91	18.7	5.1	MB	ISCCD/ISC
9 Aug 1987	21:15:03	29.47	83.74	–	5.5	MB	ISCCD/ISC
16 Jul 1986	22:03:07	31.05	78.00	4.4	5.1	MS	ISCCD/ISC
6 Jul 1986	19:24:23	34.45	80.20	9.0	5.7	MB	ISCCD/ISC
26 Apr 1986	07:35:16	32.15	76.40	33.0	5.2	MS	ISCCD/ISC
18 Nov 1984	22:04:36	28.67	83.32	–	5.4	MB	ISCCD/ISC
18 May 1984	04:28:52	29.52	81.79	–	5.6	MB	ISCCD/ISC
14 Mar 1984	15:32:33	34.23	79.63	22.2	5.1	MB	ISCCD/ISC
14 Mar 1984	01:32:11	29.18	81.12	14.8	5.0	MB	ISCCD/ISC
19 Feb 1984	15:46:26	29.84	80.54	21.0	5.1	MB	ISCCD/ISC
27 Feb 1983	20:33:07	32.60	78.57	40.0	5.3	MB	ISCCD/ISC
25 Jan 1982	17:26:17	31.58	82.25	33.0	5.1	MB	ISCCD/ISC
23 Jan 1982	17:48:02	31.56	82.21	30.9	5,3	MB	ISCCD/ISC
23 Jan 1982	17:37:29	31.68	82.28	25.0	6.0	MB	ISCCD/ISC
13 Jun 1981	00:56:57	31.82	78.46	33.0	5,0	MB	ISCCD/ISC
28 May 1981	23:14:05	31.83	78.44	–	5.2	MB	ISCCD/ISC
15 May 1981	17:22:43	29.46	81.93	33.0	5.1	MB	ISCCD/ISC

HESSD
9, 541–594, 2012

Table A1. Continued.

Date	Time	Latitude	Longitude	Depth	Magnitude	Type	Catalog
13 May 1981	02:07:52	32.58	82.36	–	5.0	MB	ISCCD/ISC
6 Mar 1981	05:58:48	29.80	80.66	23.6	5.1	MB	ISCCD/ISC
23 Aug 1980	21:50:01	32.90	75.80	12.5	5.2	MB	ISCCD/ISC
29 Jul 1980	14:58:42	29.63	81.09	–	6.5	MS	ISCCD/ISC
29 Jul 1980	12:23:08	29.34	81.21	3.0	5.7	MB	ISCCD/ISC
22 Jun 1980	14:38:53	30.13	81.77	–	5.1	MB	ISCCD/ISC
28 Dec 1979	01:59:18	30.82	78.57	23.0	5.0	MB	ISCCD/ISC
20 May 1979	22:59:12	29.93	80.27	–	5.7	MB	ISCCD/ISC
8 Aug 1978	10:12:29	32.27	83.10	3.3	5.1	MB	ISCCD/ISC
14 Jun 1978	16:12:05	32.24	76.61	6.7	5.0	MB	ISCCD/ISC
4 Apr 1978	00:40:29	32.98	82.26	–	5.5	MB	ISCCD/ISC
27 Mar 1977	05:36:49	32.67	78.66	26.0	5.1	MB	ISCCD/ISC
19 Feb 1977	06:15:25	31.80	78.43	40.0	5.4	MB	ISCCD/ISC
8 Sep 1976	20:13:01	32.03	78.76	–	5.3	MB	ISCCD/ISC
6 Jul 1976	02:55:49	32.44	78.35	24.6	5.1	MB	ISCCD/ISC
10 May 1976	18:43:53	29.33	81.46	–	5.2	MB	ISCCD/ISC
5 Feb 1976	12:04:31	31.24	77.03	5.5	5.0	MB	ISCCD/ISC
7 Jan 1976	00:24:53	32.97	76.12	40.3	5.3	MB	ISCCD/ISC
11 Dec 1975	10:09:50	33.00	76.17	42.0	5.0	MB	ISCCD/ISC
10 Dec 1975	03:26:06	32.95	76.10	4.5	5.3	MB	ISCCD/ISC
5 Dec 1975	07:37:10	33.10	76.13	23.8	5.3	MB	ISCCD/ISC
5 Nov 1975	00:35:57	32.07	78.74	21.1	5.0	MB	ISCCD/ISC
6 Sep 1975	04:44:33	29.21	81.95	–	5.1	MB	ISCCD/ISC
29 Jul 1975	02:40:51	32.57	78.49	–	5.5	MB	ISCCD/ISC
19 Jul 1975	06:10:54	31.95	78.59	–	5.1	MB	ISCCD/ISC
2 Feb 1975	19:14:10	32.55	78.50	21.0	5.1	MB	ISCCD/ISC
19 Jan 1975	08:12:10	31.94	78.52	48.6	5.8	MB	ISCCD/ISC
19 Jan 1975	08:01:58	32.39	78.50	1.4	6.2	MB	ISCCD/ISC
19 Jan 1975	08:00:18	32.30	78.66	–	5.1	MB	ISCCD/ISC
23 Dec 1974	09:45:42	29.32	81.38	45.0	5.2	MB	ISCCD/ISC
16 Dec 1973	19:09:47	34.27	74.05	40.0	5.1	MB	ISCCD/ISC

HESSD
9, 541–594, 2012

Table A1. Continued.

Date	Time	Latitude	Longitude	Depth	Magnitude	Type	Catalog
24 Oct 1973	05:23:51	33.15	75.92	36.9	5.3	MB	ISCCD/ISC
16 Jan 1973	21:31:26	33.29	75.83	39.2	5.1	MB	ISCCD/ISC
6 Sep 1972	02:51:28	32.49	78.51	14.0	5.0	MB	ISCCD/ISC
17 Aug 1972	18:14:25	30.75	78.42	33.0	5.2	MB	ISCCD/ISC
15 Mar 1972	06:00:30	30.53	84.43	–	5.1	MB	ISCCD/ISC
4 Feb 1972	14:08:22	30.34	84.47	18.0	5.1	MB	ISCCD/ISC
3 May 1971	00:33:25	30.79	84.33	–	5.3	MB	ISCCD/ISC
12 Feb 1970	01:51:48	29.24	81.57	–	5,3	MB	ISCCD/ISC
22 Jun 1969	01:33:23	30.50	79.40	–	5.3	MB	ISCCD/ISC
5 Mar 1969	11:14:58	29.46	81.02	22.0	5.0	MB	ISCCD/ISC
3 Mar 1969	06:20:21	30.04	79.84	18.0	5.1	MB	ISCCD/ISC
13 Feb 1969	06:48:36	28.50	75.70	33.0	5.1	–	ISCCD/LAO
31 May 1968	03:01:36	29.91	79.92	33.0	5.0	MB	ISCCD/ISC
11 Feb 1968	20:38:27	34.15	78.70	24.0	5.1	MB	ISCCD/ISC
5 Jan 1968	06:42:44	30.41	79.25	7.0	5.0	MB	ISCCD/ISC
18 Dec 1967	10:51:36	29.46	81.71	42.0	5.0	MB	ISCCD/ISC
20 Feb 1967	15:18:39	33.63	75.33	20.0	5.5	MB	ISCCD/ISC
21 Dec 1966	22:10:59	29.65	80.79	21.0	5.3	MB	ISCCD/ISC
16 Dec 1966	20:52:16	29.62	80.79	–	5,7	MB	ISCCD/ISC
15 Aug 1966	02:15:28	28.67	78.93	5.0	5.6	MB	ISCCD/ISC
5 Aug 1966	01:03:02	32.76	79.61	–	5.2	MB	ISCCD/ISC
29 Jun 1966	00:42:10	29.69	80.86	21.0	5.1	MB	ISCCD/ISC
27 Jun 1966	13:55:49	29.62	80.93	–	5.3	MB	ISCCD/ISC
27 Jun 1966	11:21:42	29.57	80.82	26.0	5.2	MB	ISCCD/ISC
27 Jun 1966	10:59:18	29.71	80.89	–	6.0	MB	ISCCD/ISC
27 Jun 1966	10:49:51	29.50	80.90	72.0	5.4	MB	ISCCD/ISC
27 Jun 1966	10:47:45	29.55	80.99	43.0	5.3	MB	ISCCD/ISC
27 Jun 1966	10:41:08	29.62	80.83	33.0	6.0	MB	ISCCD/ISC
6 Mar 1966	02:15:57	31.49	80.50	50.0	6.0	MB	ISCCD/ISC
6 Mar 1966	02:10:52	31.51	80.55	5.0	5.4	MB	ISCCD/ISC
11 Oct 1965	20:15:15	33.80	78.20	33.0	5.2	–	ISCCD/QUE

HESSD
9, 541–594, 2012

Table A1. Continued.

Date	Time	Latitude	Longitude	Depth	Magnitude	Type	Catalog
1 Jun 1965	07:52:25	28.59	83.06	20.0	5.3	MB	ISCCD/ISC
31 May 1965	02:04:43	32.65	77.99	28.0	5.2	MB	ISCCD/ISC
20 Apr 1965	05:15:30	33.86	82.10	89.0	5.8	MB	ISCCD/ISC
18 Mar 1965	02:41:30	29.55	80.26	67.0	5.0	MB	ISCCD/ISC
20 Dec 1964	03:31:32	29.35	81.10	9.0	5.3	MB	ISCCD/ISC
2 Dec 1964	08:21:42	29.58	81.10	3.0	5.2	MB	ISCCD/ISC
6 Oct 1964	20:19:32	29.40	80.98	11.0	5.3	MB	ISCCD/ISC
26 Sep 1964	00:46:03	29.96	80.46	50.0	5.9	MB	ISCCD/ISC
24 May 1964	00:00:48	30.04	82.18	23.0	5.1	MB	ISCCD/ISC
17 Jun 1962	00:00:00	33.74	75.83	88.0	5.5	–	HEP
10 Jul 1947	00:00:00	32.60	75.90	–	6.0	–	HEP
10 Jul 1946	00:00:00	32.60	75.90	–	6.0	–	HEP
22 Jun 1945	00:00:00	32.50	76.00	–	6.5	–	HEP
21 Nov 1939	00:00:00	36.50	74.00	–	6.9	–	HEP
28 Feb 1906	00:00:00	32.00	77.00	–	7.0	–	HEP
4 Apr 1905	00:00:00	32.30	76.20	25.0	8.0	–	HEP

HESSD
9, 541–594, 2012

Table A2. Compilation of suspended sediment flux data for some Himalayan rivers. We first list tributaries followed by their corresponding main stems in downstream direction ranging from west to east. The catchment denudation rate is based on a bulk rock density of 2.65 $g\,cm^{-3}$ and accounts only for the suspended sediment flux.

River	Location	Latitude [°]	Longitude [°]	Elevation [m]	Drainage area [km^2]	Obs. period	Runoff [$m\,yr^{-1}$]	Suspended-Sediment Load [$10^6\,t\,yr^{-1}$]	Suspended-Sediment Yield [$t\,km^{-2}\,yr^{-1}$]	Catchment denudation [$mm\,yr^{-1}$]	Reference
Shyok	Yugo	35.18	76.10	2469	33 670	1973–1998	0.33	31.1	924	0.35	Ali and De Boer (2007)
Shigar	Shigar	35.33	75.75	2438	6610	1985–1998	0.99	16.8	2542	0.96	
Hunza	Dainyor Bridge	35.93	74.38	1370	13 157	1966–1998	0.80	44.4	3373	1.27	
Gilgit	Gilgit	35.93	74.31	1430	12 095	1963–1998	0.74	6.0	498	0.19	
Gilgit	Alam Bridge	35.77	74.60	1280	26 159	1966–1998	0.78	54.8	2095	0.79	
Astore	Doyian	35.55	74.70	1583	4040	1974–1998	1.01	1.7	427	0.16	
Gorband	Karora	34.89	72.77	880	635	1975–1997	1.04	0.2	250	0.09	
Brandu	Daggar	34.50	72.46	700	598	1970–1998	0.30	0.3	442	0.17	
Siran	Phulra	34.31	73.08	732	1057	1970–1998	0.63	2.4	2306	0.87	
Siran	Thapla	34.13	72.90	440	2799	1960–1973	0.35	2.9	1024	0.39	
Indus	Kharmong	34.93	76.22	2542	67 856	1983–1998	0.23	23.9	355	0.13	
Indus	Kachura	35.45	75.42	2341	112 665	1970–1998	0.30	80.1	710	0.27	
Indus	Partab Bridge	35.73	74.62	1250	142 825	1963–1995	0.39	138.3	968	0.37	
Indus	Shatial Bridge	35.53	73.56	1040	150 220	1983–1998	0.42	118.6	789	0.30	
Indus	Barsin	35.30	73.27	780	157 600	1974–1979	0.36	140.5	892	0.34	
Indus	Besham Qila	34.92	72.88	580	162 393	1969–1998	0.47	194.4	1197	0.45	
Indus	Darband	34.36	72.84	440	166 154	1960–1973	0.47	287.6	1731	0.65	
Chandra	Ghousal	32.53	76.96	2850	2490	1978–1995	–	1.3	513	0.19	Rao et al. (1997)
Bhaga	Tandi	32.54	76,98	2846	1530	1977-95	–	0.6	371	0.14	
Marusudar	Tillar	33.57	75.79	2066	2800	1968–1987	–	1.0	373	0.14	
Marusudar	Sirshi	33.46	75.86	1620	3335	1968–1995	–	3.1	939	0.35	
Marusudar	Kuriya	33.35	75.73	1106	3960	1968–1989	–	3.5	878	0.33	
Chenab	Benzwar	33.36	75.74	1135	10 040	1972–1995	–	16.0	1597	0.60	
Chenab	Premnagar	33.15	75.70	886	15 490	1968–1995	–	21.1	1363	0.51	
Chenab	Dhamkund	33.24	75.14	600	18 750	1968–1995	–	35.6	1900	0.72	
Chenab	Akhnoor	32.89	74.74	305	21 808	1971–1995	–	22.4	1029	0.39	
Spiti	Khab	31.81	78.64	2550	12 477	2005–2008	0.26	6.2	499	0.19	this study
Baspa	Sangla	31.42	78.26	2550	989	2004–2008	1.14	1.7	1717	0.65	
Wanger	Kafnu	31.62	78.02	2450	310	1999–1905	1.72	0.2	614	0.23	
Ganvi	Ganvi	31.56	77.75	1730	117	2003	1.27	0.2	1507	0.57	
Sutlej	Khab	31.80	78.64	2550	30 950	2005–2008	0.07	6.9	223	0.08	
Sutlej	Jangi	31.63	78.43	2310	44 732	2007	0.15	13.5	302	0.11	
Sutlej	Karchham	31.50	78.19	1820	46 438	2006–2007	0.16	25.8	556	0.21	
Sutlej	Wangtoo	31.56	77.98	1480	48 316	2004–2009	0.20	29.7	615	0.23	
Sutlej	Suni	31.24	77.12	645	52 983	1994–1996	–	36.9	686	0.26	Jain et al. (2003)
Sutlej	Kasol	31.38	76.88	520	53 768	1994–1996	–	43.2	816	0.31	
Yamuna	Tajewala	30.32	77.58	370	9572	1983	1.10	18.1	1889	0.71	Jha et al. (1988)
Bhagirathi	Maneri	30.74	78.54	1295	4024	2004	1.22	3.7	917	0.35	Chakrapani et al. (2009)
Alaknanda	Srinagar	30.23	78.77	524	10 237	2004	1.70	10.2	995	0.38	
Ganga	Rishikesh	30.07	78.29	330	20 600	2004	1.15	12.9	628	0.24	

Discussion Paper | Discussion Paper | Discussion Paper | Discussion Paper |

HESSD

9, 541–594, 2012

Climatic controls on suspended sediment flux in the Sutlej River Valley

H. Wulf et al.

Table A2. Continued.

River	Location	Latitude [°]	Longitude [°]	Elevation [m]	Drainage area [km^2]	Obs. period	Runoff [$m\,yr^{-1}$]	Suspended-Sediment Load [$10^6\,t\,yr^{-1}$]	Suspended-Sediment Yield [$t\,km^{-2}\,yr^{-1}$]	Catchment denudation [$mm\,yr^{-1}$]	Reference
Dudh Khola	Dudh	28.52	84.36	2000	491	2001–2004	0.67	0.2	508	0.19	Gabet et al. (2008)
Khudi Khola	Khudi	28.28	84.35	820	152	2000–2005	3.54	0.5	3392	1.28	
Marsyandi	Koto	28.55	84.25	2640	812	2001–2004	0.76	1.4	1696	0.64	
Marsyandi	Nar	28.55	84.26	2650	1052	2001–2003	0.15	0.2	170	0.06	
Marsyandi	Upper Dharapani	28.53	84.35	2030	1946	2001–2003	0.56	1.3	678	0.26	
Marsyandi	Lower Dharapani	28.51	84.36	1880	2605	2001–2002	0.44	2.2	848	0.32	
Marsyandi	Bhulbule	28.28	84.36	788	3217	2001–2003	0.76	2.7	848	0.32	
Gandak	Triveni	27.43	83.90	110	37 845	1980–1989	1.53	78.5	2074	0.78	Sinha and Friend (1994)
Brahmaputra	Pasighat	28.08	95.34	150	249 000	–	0.80	210.0	843	0.32	Stewart et al. (2008)

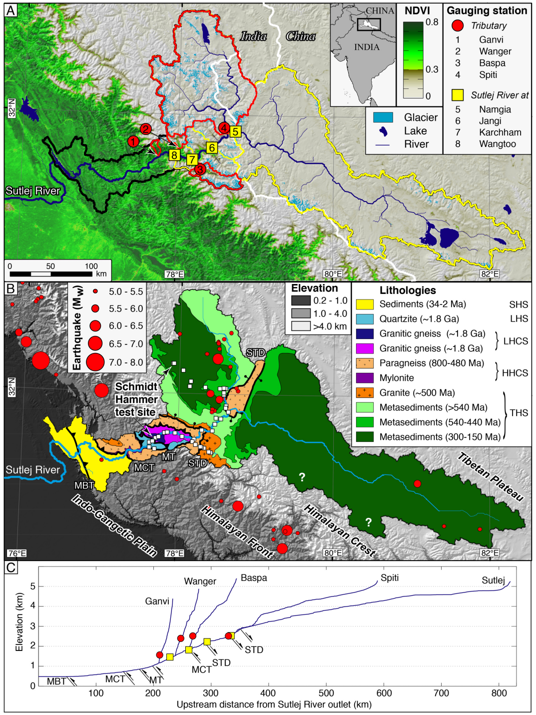

Fig. 1. **(A)** Map of the study area, showing the normalized difference vegetation index (NDVI) (Huete et al., 2002), draped over a shaded relief map, and overlain by glaciers, lakes, and the Sutlej River network. Numbers denote gauging stations where river discharge and suspended sediment concentration was measured. The corresponding upstream areas of the Sutlej River and its tributaries are indicated in red and yellow, respectively. **(B)** Geologic formations and fault systems (modified after Thiede et al., 2004; Vannay et al., 2004; Webb et al., 2011) within the study area together with locations of Schmidt hammer test sites and earthquake locations (http://www.iris.washington.edu) (Table A1). Lithologies are grouped into the Sub-Himalaya Sequence (SHS), Lesser Himalayan Sequence (LHS), Lesser Himalayan Crystalline Sequence (LHCS), Higher Himalayan Crystalline Sequence (HHCS), and Tethyan Himalayan Sequence (THS). Major tectonic faults along the Sutlej River are indicated by the following abbreviations: MBT (Main Boundary Thrust), MCT (Main Central Thrust), MT (Munsiari Thrust), STD (South Tibetan Detachment). Surrounding areas show elevation draped over shaded-relief map. **(C)** Longitudinal river profile of the Sutlej River and its tributaries analyzed in this study. Red circles and yellow squares denote gauging station location as indicated in 1A.

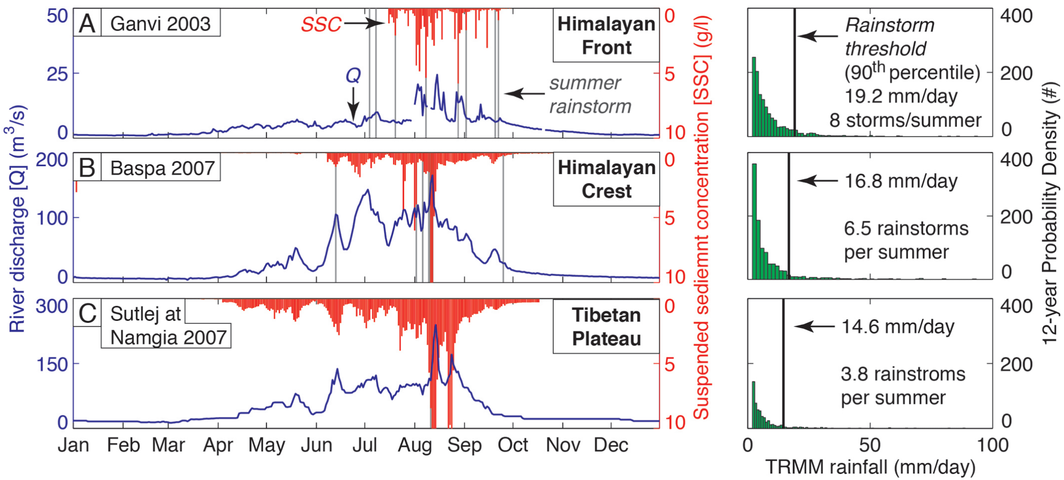

Fig. 2. Annual course of river discharge (*Q*) and suspended sediment concentration (SSC) underlain by summer rainstorms (May–October) in different orogenic regions represented by the Ganvi tributary during the year 2003 **(A)**, the Baspa tributary during 2007 **(B)**, and the Sutlej River at Namgia during 2007 **(C)**. Panels on the right show the catchment-respective probability density (number of occurrences) of wet rainfall days ≥2 mm in 1 mm day^{-1} bins as taken from the 12-year TRMM 3B42 time series. Note that SSC data in **(A)** is restricted to 77 days form mid July to mid September.

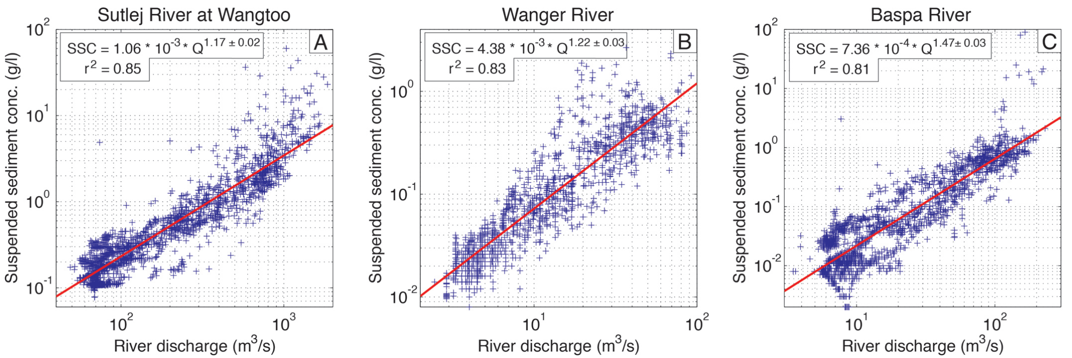

Fig. 3. Sediment rating curves for the Sutlej River at Wangtoo **(A)**, the Wanger River **(B)**, and the Baspa River **(C)** showing suspended sediment concentration (SSC) as a function of daily river discharge (Q). Note the different scales of the axes.

HESSD
9, 541–594, 2012

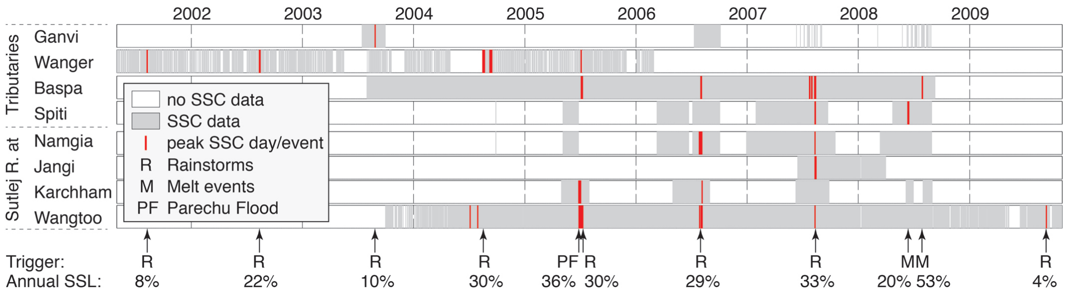

Fig. 4. Time series of peak SSC days/events within the Sutlej catchment. Plausible triggers that are related to peak SSC days/events and catchment-average percentages on the annual suspended sediment load (SSL) are indicated at the bottom. PF (Parechu Flood) is a rain-on-snow event that led to the breach of a landslide dam and caused significant flooding downstream.

HESSD
9, 541–594, 2012

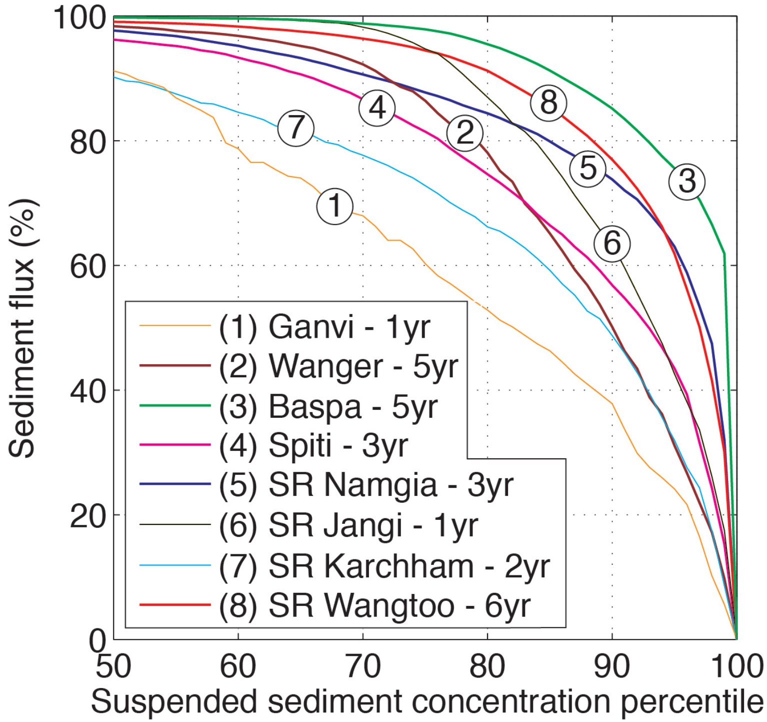

Fig. 5. Percentage of peak SSC events on total suspended sediment flux. Length of the time series is given in the legend. The legend shows tributary stations (1–4) from south to north and the Sutlej River (SR) mainstem stations (5–8) in downstream direction (cf. Fig. 1).

HESSD
9, 541–594, 2012

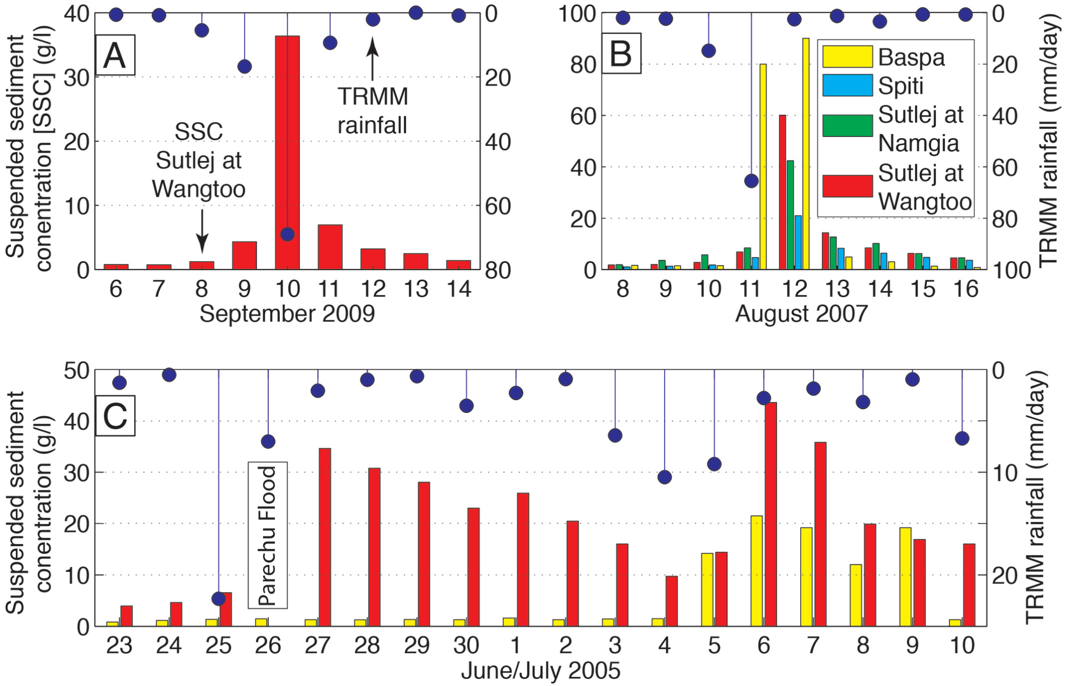

Fig. 6. Relation between peak SSC events and rainfall. **(A)** Peak SSC event triggered by a 2-day rainstorm (>90th percentile) during September 2009. Daily rainfall amounts are derived from TRMM 3B42 averaged over the Sutlej catchment at Wangtoo. **(B)** Peak SSC event caused by a synoptic rainstorm affecting several catchments in the Sutlej Valley during August 2007. Larger catchments (e.g. Spiti) show longer response times. Color coding indicates location of SSC measurements. **(C)** SSC response of the Sutlej River at Wangtoo to the lake outburst flood (Parechu Flood during June/July 2005) and a successive rainstorm, which especially affected SSC levels in the Baspa River.

HESSD
9, 541–594, 2012

Climatic controls on suspended sediment flux in the Sutlej River Valley

H. Wulf et al.

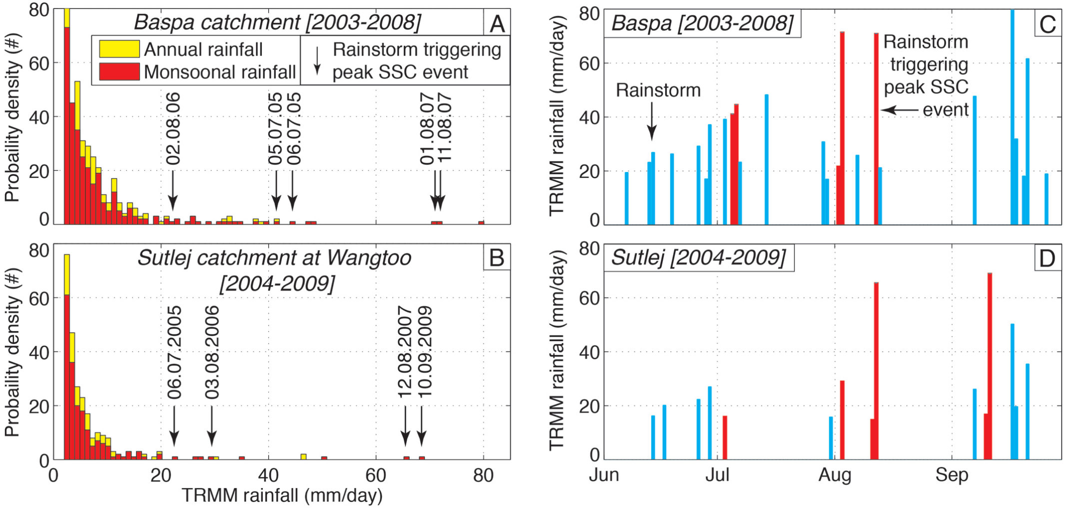

Fig. 7. Histograms of daily TRMM 3B42 data displaying annual and monsoonal (June-September) rainfall during the given time period for the Baspa catchment **(A)** and the Sutlej catchment at Wangtoo **(B)**. Arrows indicate rainstorms (≥90th rainfall percentile), which are associated with peak SSC days (99th SSC percentile). Panel **(C)** and **(D)** represent the 6-year time series of rainstorms and their impact on peak SSC days during the monsoonal period for the Baspa catchment and Sutlej catchment at Wangtoo, respectively.

HESSD
9, 541–594, 2012

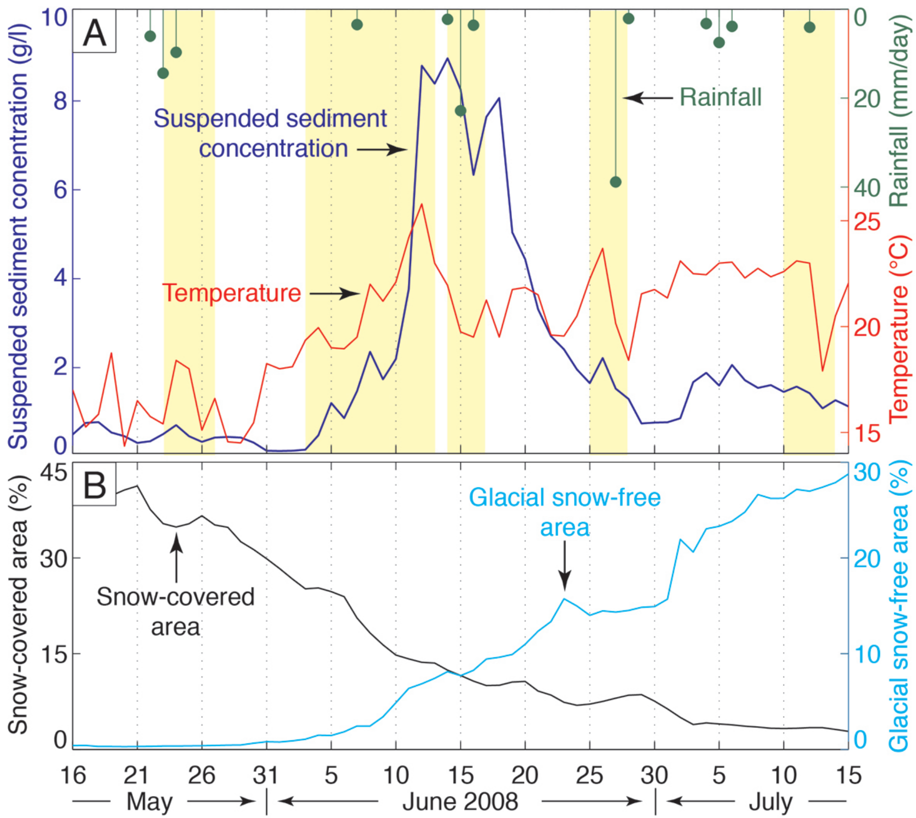

Fig. 8. (A) Spatial gradients in runoff, suspended sediment concentration (SSC), and suspended sediment yield (SSY) for the Sutlej River and tributary catchments. Correlations are weighted by the number of measurement years. The correlation is based on the catchment-average downstream distance to the Sutlej River outlet to account for the predominant catchment area location. **(B)** Conceptual model of the spatial distribution of SSC, runoff, and SSY from the Tibetan Plateau to the Himalayan Crest and the Himalayan Front.

HESSD
9, 541–594, 2012

Climatic controls on suspended sediment flux in the Sutlej River Valley

H. Wulf et al.

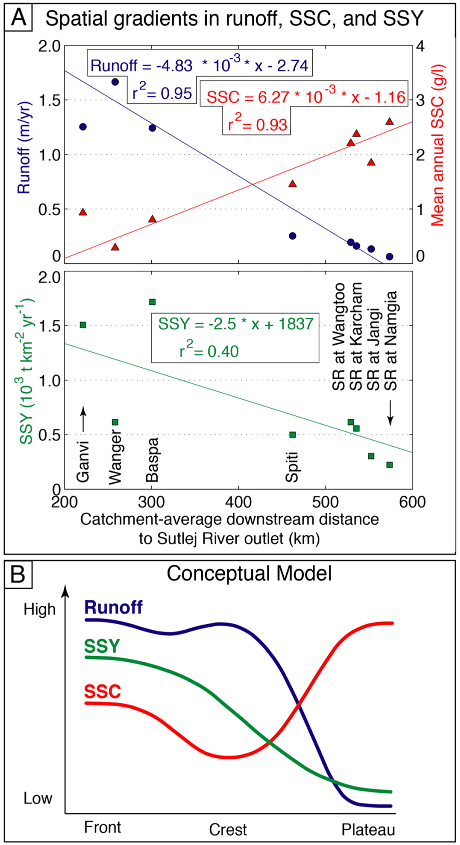

Fig. 9. Time series of daily river discharge and suspended sediment concentration data separated by month of Sutlej River at Wangtoo **(A)** and the Wanger River **(B)** covering five and six years, respectively. Hysteresis loops of the mean monthly suspended sediment flux in the Sutlej River at Wangtoo **(C)** and the Wanger River **(D)**. The error bars represent the daily standard deviation ($\pm 1\,\sigma$) of the monthly river discharge and SSC mean, respectively.

HESSD
9, 541–594, 2012

Title Page
Abstract | Introduction
Conclusions | References
Tables | Figures
◀| |▶
◀ ▶
Back | Close
Full Screen / Esc
Printer-friendly Version
Interactive Discussion

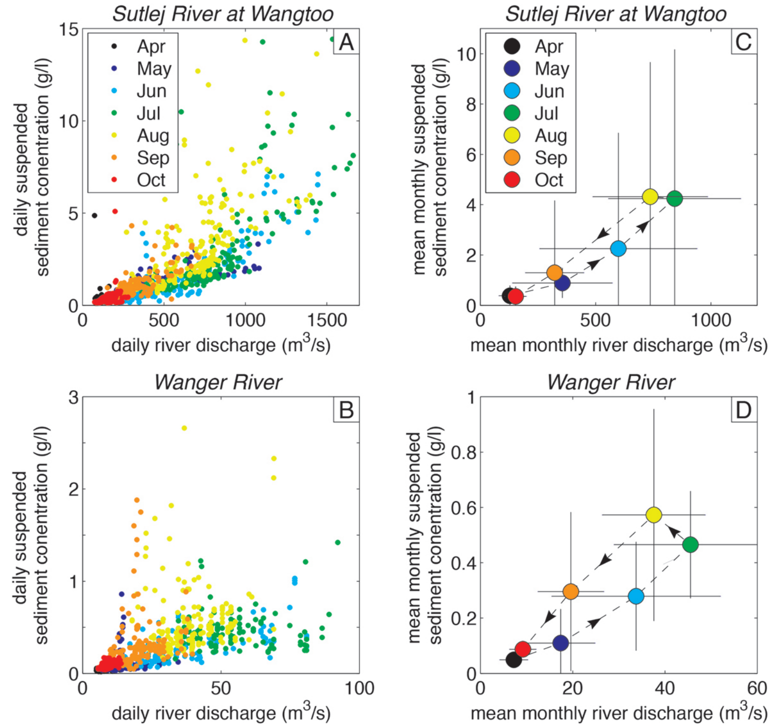

Fig. 10. Boxplots of Schmidt hammer rebound values of different rock types in parts of the Lesser Himalayan Sequence (LHS), Lesser Himalayan Crystalline Sequence (LHCS), High Himalayan Crystalline Sequence (HHCS), and Tethyan Himalaya Sequence (THS). Numbers of individual Schmidt hammer measurements are given in circles. The color codes below each rock type indicate the approximate location or lithostratigraphic group (cf. Fig. 1b). The numbers in color code of the HHCS refer different locations: (1) Karchham, (2) Leo Pargil, (3) Baspa. On each yellow box, the central red mark is the median, the edges of the box are the 25th and 75th percentiles, the whiskers extend to the most extreme data points not considered outliers, and outliers are plotted in separate red crosses.

HESSD
9, 541–594, 2012

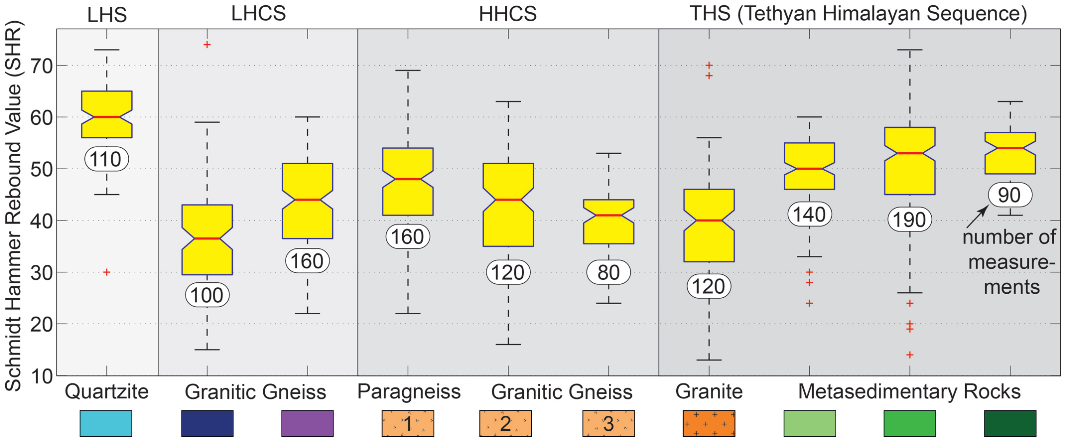

Fig. 11. (A) Comparison of SSC in the Spiti River with TRMM 3B42 rainfall averaged over the Spiti catchment and mean daily air temperature data from Namgia (cf. Fig. 1a) during a two-month period in 2008. Yellow background indicates periods of positive correlation ($r^2 = 0.68$) between SSC and temperature variations. **(B)** Percentage of snow-covered area and the percentage of glacial snow-free area in the Spiti catchment for the same period.

HESSD
9, 541–594, 2012

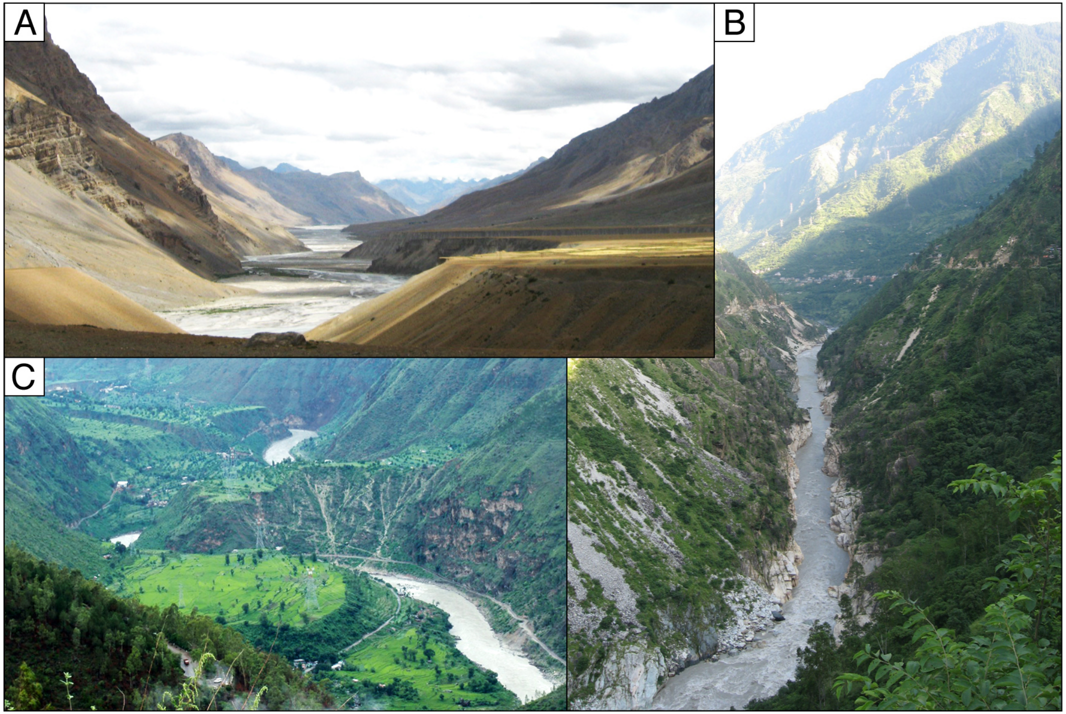

Fig. 12. Images of varying sediment storage in the Sutlej River Valley. **(A)** Fluvial terrace and alluvial fans along the high-elevated Spiti River, a major tributary to the Sutlej. **(B)** Incised bedrock along the steep middle Sutlej River section upstream of Rampur (cf. Fig. 1b) at the Himalayan Crest. **(C)** Extensive fluvial terraces along the moderately inclined lower Sutlej River section downstream of Rampur at the main Himalayan Front (cf. Bookhagen et al., 2006).

HESSD
9, 541–594, 2012

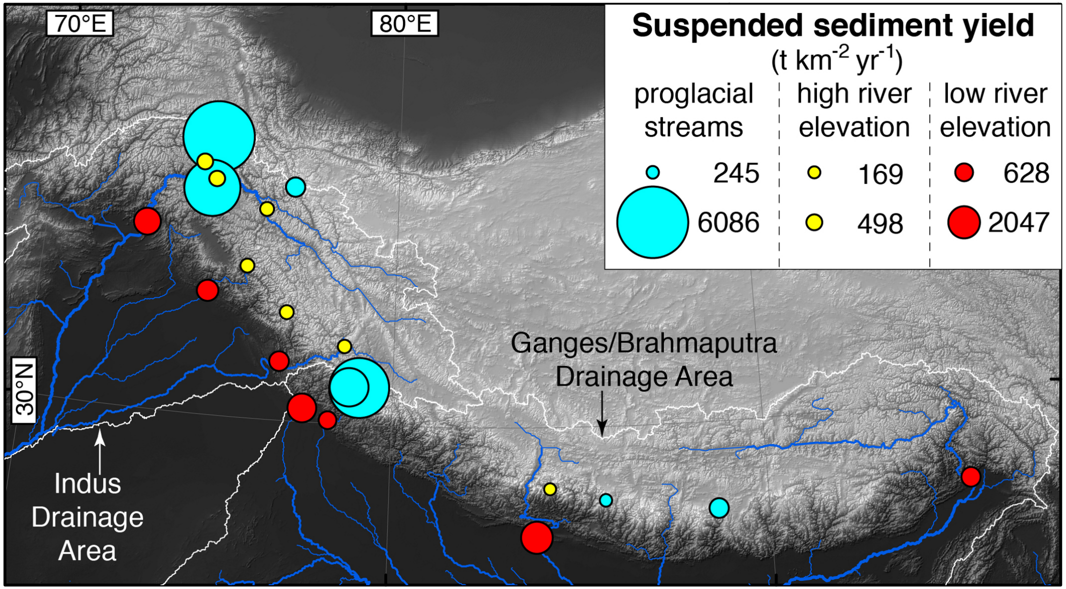

Fig. 13. Compilation of mean annual suspended sediment yield measurements in proglacial streams (>2500 m a.s.l.), upstream river catchments (>2000 m a.s.l.), and at outlet locations of major rivers (100–600 m a.s.l.). Data and respective references are given in Tables 4 and A2.